J Mater Sci (2022) 57:19212–19242

Review

Additive manufacturing of ceramic particle-reinforced aluminum-based metal matrix composites: a review

Yusuf Karabulut[1,*] and Rahmi Ünal[1]

[1] *Department of Mechanical Engineering, Gazi University, Maltepe-Ankara, Turkey*

Received: 22 July 2022
Accepted: 12 October 2022
Published online: 27 October 2022

ABSTRACT

Laser powder bed fusion (LPBF) is one of the most widely used additive manufacturing methods for fabricating metal components. It is possible to produce multi-material structures and functionally graded materials with LPBF. The usability of powder mixtures provides a great potential for the production of metal matrix composites (MMCs) with advanced mechanical properties. Among the wide variety of MMCs, aluminum matrix composites are highly potential candidates for aerospace, automotive and biomedical applications due to their outstanding properties including high wear resistance, better chemical inertness and excellent mechanical properties at elevated temperature. Therefore, in this study, ceramic particle-reinforced Al-based MMCs produced by LPBF method are reviewed for the recent developments. Feedstock preparation methods for MMCs are emphasized. The effects of reinforcement particle properties and LPBF process parameters on the microstructure, densification behavior, hardness and tensile properties are discussed comprehensively. The strengthening mechanisms that occur with the addition of ceramic reinforcement are examined. Summary of the findings from this review and trends for future research in the development of Al-based MMCs by LPBF are addressed in the final section.

Introduction

In recent years, laser powder bed fusion (LPBF) has become an emerging additive manufacturing (AM) technique that allows the production of complex parts. In the LPBF methods, parts are fabricated layer by layer based on computer-aided design (CAD) models [1]. This layered structure enables for much greater design freedom with almost no geometric restrictions. Therefore, AM is highly promising for many high-value industries such as aerospace, automotive, defense and biomedical that require high-performance products [2–5].

LPBF methods have a lot of advantages over conventional manufacturing techniques. AM

Handling Editor: David Cann.

Address correspondence to E-mail: yusufkarabulut@gazi.edu.tr

https://doi.org/10.1007/s10853-022-07850-0

technologies offer the advantages of direct production, design and processing flexibility, near-zero material wastage and net-shaped fabrication without requiring expensive molds and tools [6, 7]. Due to the complex geometry of the components used in the aerospace and automotive industries, LPBF methods can provide an extraordinary opportunity to reduce assembly cost, especially for these industries. LPBF methods can be rapidly used to investigate the manufacture of components used in specific applications with new materials. Components redesigned by designers with topology optimization can be produced easily and quickly with LPBF methods [8]. It is possible to produce multi-material structures and functionally graded materials with LPBF [9–11]. As part production in LPBF methods relies on rapid melting and solidification processes, parts have substantially refined microstructures and therefore high hardness and strength [12, 13]. The usability of powder mixtures provides a great potential for the production of metal matrix composites (MMCs) with advanced mechanical properties. However, there exist several significant challenges that adversely affect the properties of additively manufactured parts such as high porosity and surface roughness [14], high residual stress [15] and non-uniform microstructure [16]. Several post-processing operations have been adopted to enhance the surface and mechanical properties [17]. Among these post-processes, especially heat treatment and hot isostatic pressing (HIP) are utilized effectively to reduce the porosity and residual stresses in the material structure [18, 19].

Composites are consisting of two or more components that show the characteristics of a single material, but are chemically different from each other. By producing composites, it is possible to obtain some properties that cannot be obtained when the materials used alone. MMCs consist of a mixture of metal matrix and ceramic reinforcements and are also known as ceramic-reinforced metal matrix composites. MMCs have many superior properties compared to traditional metals such as better thermo-mechanical properties, excellent chemical inertness, high wear resistance, low coefficient of thermal expansion and better fatigue resistance [20–23]. Because of these superior properties, they are used in extreme operating conditions such as high load, high temperature and extensive wear operations [24–27]. MMCs are widely used in aerospace, biomedical, electronics and various engineering applications [28–30]. Various methods such as powder metallurgy [31], squeeze casting [32] and stir casting [33, 34] are used to fabricate particle-reinforced MMCs. However, these techniques, which require expensive and special tools, are insufficient, especially in the production of complex-shaped components. In addition, due to the high hardness and melting point of the manufactured components, it is very difficult to process with traditional machining techniques [35, 36]. LPBF methods have opened up new opportunities in the production and development of MMCs, thanks to their advantages over traditional manufacturing methods.

This study is a comprehensive literature review on the production of particle-reinforced MMCs by LPBF methods. Within the scope of the study, research studies in which Al alloys were used as matrix and different ceramics as reinforcing particles are examined. The microstructural properties, densification behavior and mechanical properties of ceramic particle-reinforced MMCs are compiled and discussed in detail.

Laser powder bed fusion for fabricating MMCs

Metal additive manufacturing methods such as LPBF, directed energy deposition (DED) and electron beam melting (EBM) are potential promising alternatives in the production of metal matrix composites. Among these methods, it is possible to produce highly dense AMCs with minimal defects by overcoming the problems encountered in conventional processing with the LPBF method [37]. LPBF offers significant variety for the processing of various powder materials. During the laser melting process, new constituents can be formed between the melted powders, allowing different materials to be obtained from the initial powder mixtures. The laser used to fuse the powders also triggers chemical reactions and as a result, secondary phases are formed in the part. In this complex process, it is possible to produce complex-shaped composites with a uniform distribution of secondary phases. Compared to the LPBF method, the high layer thickness and low internal cooling rate in the DED method cause the formation of coarse microstructure and high porosity in the built part [38, 39]. In the LPBF method, rapid melting and

solidification rates provide fine microstructures and thus high mechanical properties. Moreover, higher accuracy and better surface quality are obtained in the LPBF method compared to other metal AM techniques [40].

LPBF methods are classified into three basic categories: selective laser sintering (SLS), selective laser melting (SLM) and direct metal laser sintering (DMLS) [41]. DMLS is a trademark of EOS and is often used to describe SLM [42]. In SLS, metal powders are sintered with a focused laser at a temperature below the melting temperature of the powder [43]. Since the melting temperature does not have to be reached, alloys containing materials with different melting points can be easily produced. On the other hand, in the SLM method, metal powders are completely melted, resulting in a homogeneous part [44]. The schematic representation of the LPBF method is presented in Fig. 1.

Part production in the LPBF method includes the following steps:

- A powder layer of a certain thickness (typically 0.3–0.6 μm) is spread over the build platform.
- A laser fuses the first powder layer of the model.
- A new powder layer is spread over the melted powder layer using a roller.
- Further layers are fused and added.
- The process is repeated until the entire model is built.

There are several parameters that control the processing and directly affect the part quality in the LPBF. Various parameters such as process parameters (laser power, scanning speed, layer thickness, hatch distance, scanning strategy, etc.), material parameters (powder morphology, powder size, powder shape, etc.) and machine characteristics (laser type, atmosphere, etc.) should be chosen carefully. Appropriate selection of these parameters is essential to reduce internal defects inside parts [45].

LPBF has become an alternative method in composite production as it allows the use of powder mixtures as feedstock. In recent years, many research works have been carried out examining the composite production process by using LPBF. There are very few studies on the fiber-reinforced MMCs in the literature [46, 47], and these studies have generally focused on particle-reinforced MMCs. Therefore, this paper covers the emerging research on ceramic particle-reinforced Al-based MMCs.

Preparation of composite feedstock

Composite powder feedstock is required as starting material in the production of MMCs with LPBF. Size, morphology, weight/volume ratio and dispersion pattern of composite powders play significant role in determining part quality. Feedstock preparation with matrix material and particle reinforcements can be carried out with different methods such as regular mixing [48], ball milling [49], flux-assisted synthesis [50], agent-assisted deposition [51] and electroless plating [52], which of these methods chosen is of vital importance for the composite powder properties and the resulting part quality. Regular mixing and ball

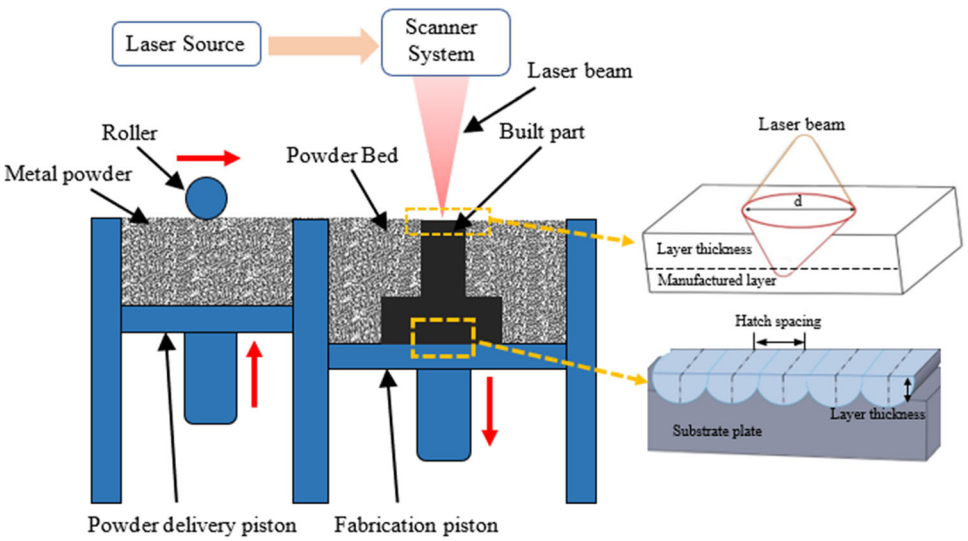

Figure 1 Schematic representation of the LPBF method.

milling methods have attracted a great deal of attention in recent years due to their higher practicality, time and cost efficiency, and applicability to a wide range of materials, and are therefore known as the most applicable processes for the preparation of composite powders. Regular mixing and ball milling methods are schematically presented in Fig. 2.

The part quality is closely related to the powder morphology in LPBF. Spherical powders are spread more uniformly on the build platform with the recoater blade during production. For this reason, spherical powders produced by gas atomization [53, 54] and plasma atomization [55–57] are mostly used in the LPBF method. Distortion of the spherical shape of the powders in the preparation of composite feedstock adversely affects the part quality. Figure 3 shows the spherical deformity of the TiN/AlSi10Mg composite feedstock prepared by wet ball milling followed by ultrasonic mixing [19]. In all feedstock preparation methods, the spherical shape of the powders is generally distorted, but mechanical mixing methods such as regular mixing and ball milling attract attention and are frequently used due to their time and cost efficiency and applicability to various materials [58]. A summary of the studies using ball milling and regular mixing methods is presented in Table 1. Han et al. [59] investigated the effect of milling and pause duration on the fabrication of ball-milled Al/Al_2O_3 composite feedstock. They found that a combination of the short milling (10 min) and long pause (15 min) duration is suitable for preparation of composite feedstock.

Whether the prepared composite feedstock is suitable for LPBF is determined using some metrological and analytical techniques. Composite powder flowability plays an important role in the uniform laying of powders on the powder bed in the LPBF method. Good-flowing powders generate powder layers with continuous and uniform thickness, reducing the detrimental dimensional effects and providing better mechanical properties [60]. The Carr index and Carney or Hall flow testing methods can be used to evaluate the flow behavior of composite feedstock. Powders with a Carr index of $< 15\%$ are considered to have good flowability.

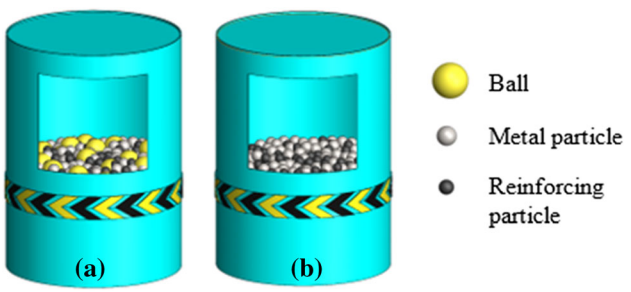

Figure 2 Schematic representation of **a** ball milling and **b** regular mixing processes.

The suitability of prepared composite feedstock for LPBF also directly depends on the morphology and size distribution of the powders, and the homogeneous mixing of the reinforcement and the matrix [61]. Powders that retain their spherical shape are more suitable for LPBF because they increase powder flowability and small particles provide uniform layer thickness. Powders morphology can be determined by analyzing powders under scanning electron microscope (SEM) and optical microscope. Particle size analyzers can be used to evaluate powder size distribution, and whether the reinforcements are uniformly dispersed in the matrix can be determined by SEM and transmission electron microscope (TEM) analyses.

Matrix materials and reinforcement particles

With LPBF method, MMCs are produced with a wide variety of matrices including Al [62], Ti [63], Fe [64, 65] Cu [66, 67] and Ni [68] and reinforcing elements including carbides (WC, SiC, B_4C, TiC) [69], oxides (Fe_3O_4, ZrO_2, Al_2O_3) [62, 70], nitrides (ZrN, Si_3N_4, TiN) [71, 72], borides (TiB, ZrB_2, TiB_2, WB) [73] and different forms of carbon (graphite, carbon nanotubes, graphene) [74]. Among these, Al as a matrix material and ceramic particles such as SiC, TiC, TiN, TiB_2 and Al_2O_3 as particle reinforcements are the most frequently used [75, 76].

In composite materials, the relationship between the matrix and the reinforcing particles is one of the most significant factors determining the composite properties. The chemical composition, type, shape and size of the reinforcing particles determine the functionality of the composites. Therefore, the selection of reinforcing particles is very crucial. In the following sections, research works using Al and Al alloys as matrix material and ceramic particles as reinforcements are extensively studied.

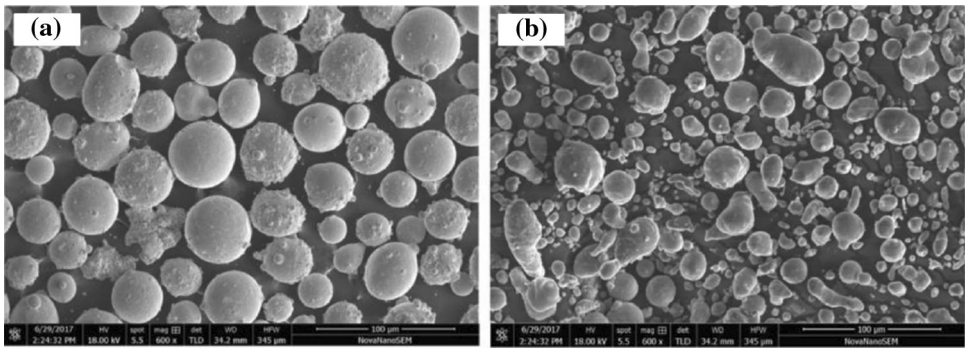

Figure 3 **a** Pure AlSi10Mg powders and **b** nTiC/AlSi10Mg composite powders after wet ball milling followed by ultrasonic mixing [19].

Table 1 Summary of the literature review of the studies using ball milling and regular mixing methods to prepare composite feedstock

Matrix	Reinforcement	Ball-to-powder weight ratio	Rotational speed (rpm)	Duration (h)	References
Al	SiC	1:1	10	12	[154]
AlSi7Mg	SiC	–	100	3	[93]
AlSi10Mg	SiC	2:1	80	2	[91]
AlSi10Mg	SiC	2:1	80	2	[88]
AlSi10Mg	SiC	1:1	200	4	[92]
Al-12Si	SiC	-	100	30 min	[87]
AlSi10Mg	SiC	1:1	200	4	[90]
AlSi10Mg	SiC	1:1	200	2 (15 min. milling and 5 min. pause)	[155]
AlSi10Mg	TiCN	–	–	4	[156]
Al-15Si	TiC	–	240	4	[111]
AlSi10Mg	TiC	1:1	200	4	[123]
Al-12Si	TiB_2	10:1	100	2	[147]
AlSi10Mg	Al_2O_3	1:1	600	5	[144]
Al	Al_2O_3	10:1	200	16 (30 min. milling and 10 min. pause)	[136]
AlSi10Mg	Graphene nanoplatelets	8:1	230	4 (20 min. milling and 10 min. pause)	[157]
AlSi10Mg	Carbon nanotube	2:1	300	4	[158]
AlSi10Mg	Al_2O_3	10:1	70	4	[135]

Reinforced by SiC particles

SiC is one of the most widely used ceramic particle reinforcements in the production of MMCs by the LPBF method. SiC is preferred due to its compatibility with Al-based matrix material and its superior properties [77–80]. The basic physical properties of SiC are listed in Table 2 [81, 82]. SiC particle-reinforced MMCs are typical candidate materials in the aerospace, automotive and military industries due to their high strength, high hardness and modulus, and high corrosion and wear resistance [83].

Microstructural characterization

When the composite feedstock prepared with SiC and Al powders is irradiated by laser beam, Al powders melt completely, while SiC particles partially melt or do not melt due to the high melting temperature. SiC particles come into contact with liquid Al and intense chemical reactions occur between SiC and liquid Al, and new phases are formed as a result of these reactions. When the powder bed temperature exceeds 1670 K, the following reaction occurs:

Table 2 Basic physical properties of SiC [81, 82]

Elastic modulus	Flexural strength	Hardness	Poisson's ratio	Density
410 GPa	359 MPa	2563 HV	0.16	> 3.1 g/cm^3

$$4Al + 4SiC \rightarrow Al_4SiC_4 + 3Si \quad (1)$$

Another reaction that occurs when the temperature exceeds 940 K [84]:

$$4Al + 3SiC \rightarrow Al_4C_3 + 3Si \quad (2)$$

In order to evaluate the microstructure of SiC-reinforced Al matrix composites produced by LPBF, it is necessary to analyze the reactions occurring at the interface well. There are two theories to explain the reaction mechanisms between SiC and Al matrix: melting theory and reaction theory [85, 86]. The melting theory proposes that SiC and Al melt simultaneously and phases such as Al_4SiC_4 and Si precipitate during solidification. The reaction theory suggests that SiC particles react with molten Al at the interface and different phases are formed on the particle surface. Cons, the melting theory occurs at high temperatures, while the reaction theory occurs at low temperatures. It has been reported that the interface products formed with the combination of both theories in the LPBF method [87].

Xue et al. [88] used the LPBF method at different scanning speeds to produce SiC-reinforced AlSi10Mg composite. They found that the SiC density in the structure decreased with the decrease in the scanning speed. As the scanning speed decreases, the interaction time of the laser beams with the powders increases. The chemical reactions between SiC and liquid Al also increase, resulting in a decrease in SiC density. They also determined that the Al_4SiC_4 phase was formed at the interface and that there were no micropores and microcracks at the interface as shown in Fig. 4 [88]. The absence of micropores and microcracks at the interface indicates that the bonding between the matrix and the particle reinforcement is strong, which positively affects the mechanical properties of the composite. However, the difference in the coefficient of thermal expansion between the particle reinforcement and the matrix can sometimes cause cracks and porosities at the interfaces [89]. These cracks and porosities reduce the load transfer capacity from the matrix to the reinforcement. The increase in laser energy density due to the increase in laser power also increased the chemical reactions at the interface and caused a decrease in the SiC density in the microstructure and the formation of reaction products of Al_4C_3 [87]. The increase in laser energy density caused more decomposition of SiC in the Al matrix, which increased the reaction products [90].

Chemical reactions at the interface can also vary depending on the SiC particle size. As the SiC particle size decreases, the interfacial reactions increase and the amount of newly formed phase (Al_4SiC_4) is observed in a larger volume fraction [91, 92]. This is due to the relatively higher specific surface area of the small-sized SiC particles, thus forming a stronger bonding with the Al matrix.

With the addition of SiC reinforcement, it was observed that the average grain diameter decreased by 30.99% and SiC agglomerations were observed in some regions of microstructure [93]. SiC particles in molten pools provide a large number of nucleation sites, enabling the formation of fine recrystallized grains and restricting the growth of Al grains. In addition, as a result of XRD analyses, it was determined that Al, Si, Mg_2Si and SiC phases were formed in the microstructure, as well as nanosized reaction products Al_4C_3 phase. The different phases that occur in the microstructure of the specimen produced by the LPBF method by adding nano-SiC particles to the $AlSi_7Mg$ matrix are schematically presented in Fig. 5 [93].

Densification behavior

The densification behavior of particle-reinforced MMCs produced by LPBF method depends on many factors. These factors can be reinforcement size, fraction and shape, as well as LPBF processing parameters. In addition, the temperature in the powder bed during production is very crucial on the densification behavior. The laser absorption of the composite feedstock has a notable importance on the densification behavior of the composites, as it has a significant effect on the powder bed temperature. The porosity values of the SiC-reinforced and non-reinforced Al powders were measured as $0.25 + 0.11\%$ and $0.59 + 0.79\%$, respectively [93]. After the addition of SiC particles, the laser reflectivity decreased,

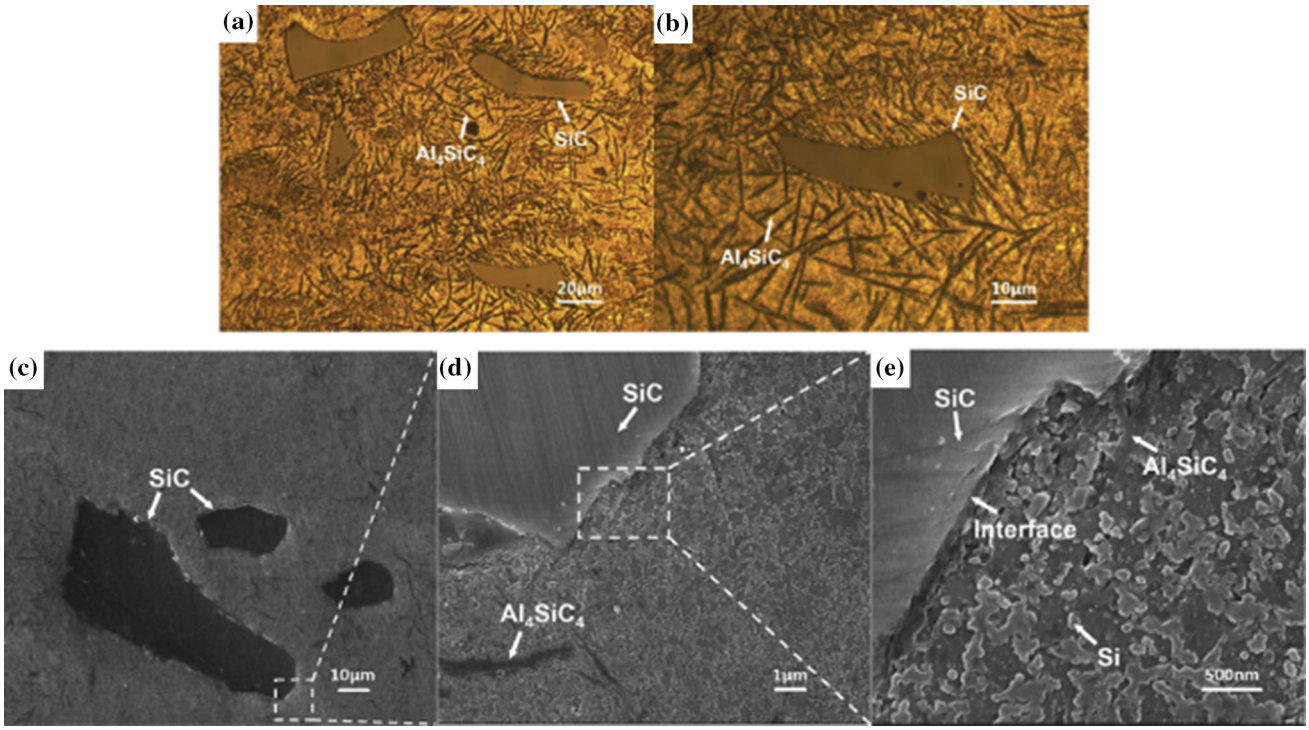

Figure 4 Optical Microscope **a**, **b** and Scanning Electron Microscope **c**, **d**, e images of the SiC-reinforced AlSi10Mg composite [88].

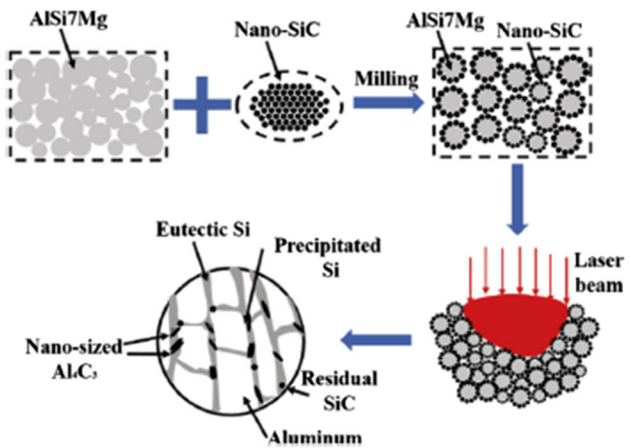

Figure 5 Schematic representation of the formation mechanism of different phases during LPBF method of $AlSi_7Mg$/nano-SiC composite [93].

that is, the laser absorption increased [94, 95]. The laser reflectivity of SiC-reinforced and non-reinforced Al alloys was determined as 31.71% and 23.05% at 1064 nm wavelength, respectively [91]. The increase in laser absorbance helped to improve the liquid–solid wettability by increasing the molten pool temperature. Moreover, increased laser absorption provides a more stable melt pool formation.

The decrease in SiC particle size significantly increases the relative density. When coarse SiC particles are used, the particles cannot interact with the laser for a sufficient time and remain in the structure almost unmelted, which limits the microstructural homogeneity. Coarse SiC particles increase the melt viscosity and cause the melting flow to be irregular. As a result, large-sized pores are formed in the structure due to the instability of the molten pool and the balling effect [92]. With the decrease in the particle size, the laser absorption of the powder mixture and thus temperature in the molten pool increase, leading to the increase in the Marangoni flow [96]. In addition, high laser absorption causes an increase in the molten pool size and a decrease in the viscosity of the blended melt [95]. Consequently, the increase in fluidity in the molten pool provides a more homogeneous distribution of SiC particles within the structure [91]. Reducing SiC particle size also increases chemical reactions at the interface. Thus, the wettability of liquid Al and SiC particles increases, preventing the formation of porosities and cracks at the particle–matrix interface.

Figure 6 shows OM and SEM micrographs and relative density of the as-built AlSi10Mg/SiC composites fabricated under different laser powers [97].

The densification rate of Al-based SiC-reinforced composites increases as the applied laser energy density increases [87, 90]. Increasing the laser power or decreasing the scanning speed elevates the molten pool temperature. With the increase in the molten pool temperature, SiC particles melt at a higher rate, reducing the viscosity. The increase in laser intensity also allows the molten pool to remain molten for a longer time, which increases the fluidity and facilitates the liquid metal flow in the molten pool. Thus, the liquid melt can easily fill the pores [98]. At high laser intensities, the molten pool temperature rise excessively, resulting in a decrease in the densification rate. Extremely high temperatures, which may exceed the boiling point, can cause vaporization of alloying elements [99]. Vaporization of volatile elements causes the formation of keyhole-shaped pores in the molten pool [97]. As discussed above, proper selection of LPBF process parameters is critical for fabricating nearly fully dense parts.

Hardness and tensile properties

The hardness and tensile properties of the Al-based MMCs produced by the LPBF method are significantly associated with the density level and microstructure. The addition of SiC particles increases the composite hardness [93]. As a result of the interfacial reactions with SiC, the precipitate phases and interfacial products are formed, which leads to the precipitation strengthening effect. In addition, the microstructure refined with SiC reinforcement is another reason for the hardness increase. According to the Hall–Patch formula, the microhardness is improved due to the grain refinement [100].

Figure 7 shows the effects of coarse, medium and fine SiC particles on microhardness and its distribution [92]. The use of coarse SiC particles enables the formation of large-sized pores in the microstructure. Moreover, the SiC particles remain nearly unmelted in the microstructure and the interfacial bonding is weak [92]. As the SiC particle size decreases, the grain size decreases and almost full density is achieved, stronger interfacial bonding is formed between SiC and Al matrix and the amount of interfacial product increases [91]. The hardness difference between the SiC-reinforced AlSi10Mg composite and the unreinforced AlSi10Mg can vary up to 40% [91, 101]. Consequently, hardness increases with the decrease in particle size can be attributed to three strengthening mechanism: precipitation strengthening, grain refinement strengthening and strong

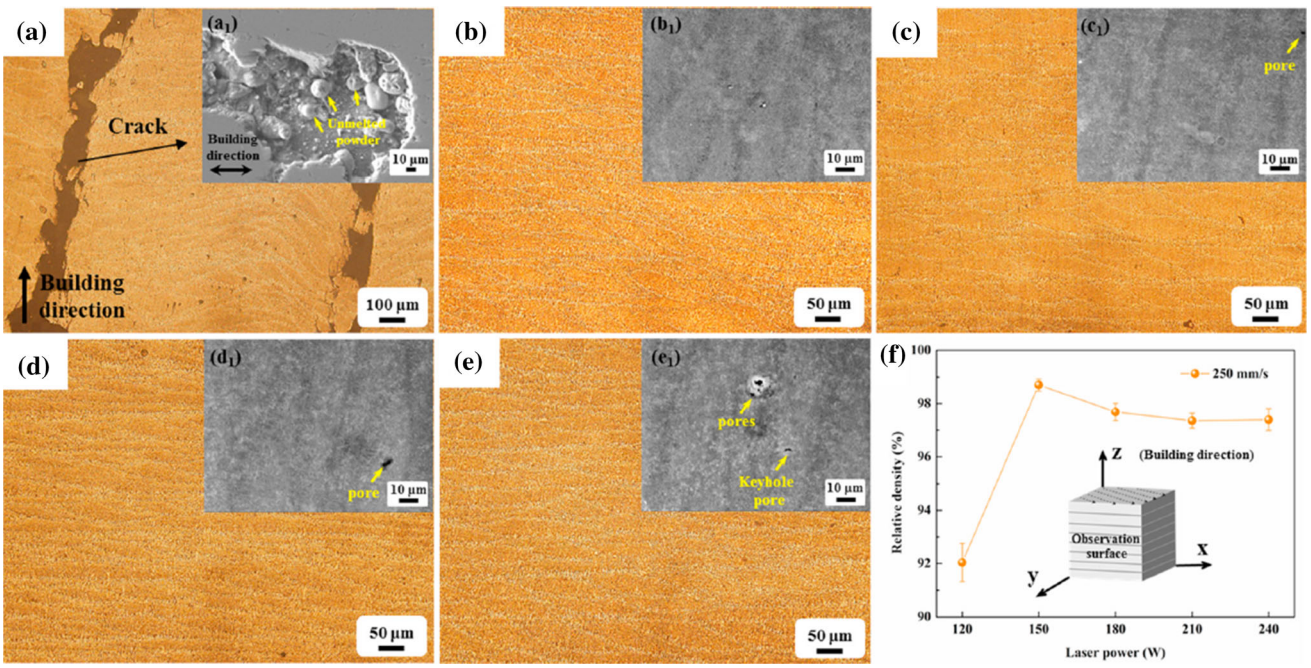

Figure 6 Optical micrographs and SEM images of as-built AlSi10Mg/SiC composites at different laser power of 120 W (**a**, a_1), 150 W (**b**, b_1), 180 W (**c**, c_1), 210 W (**d**, d_1), 240 W (**e**, e_1) and the variation of relative densities **f** [97].

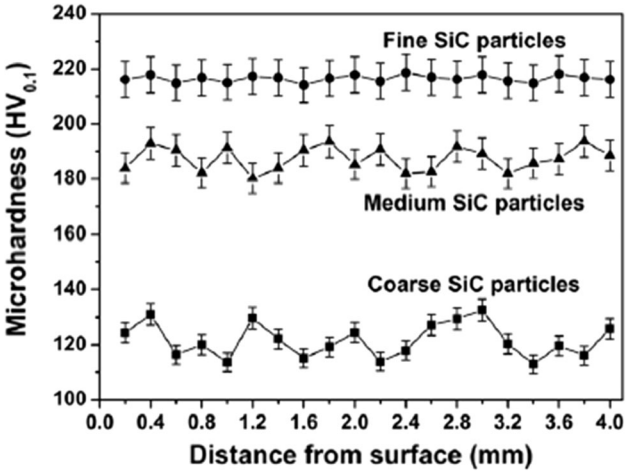

Figure 7 Effect of SiC particle size on microhardness and its distribution [92].

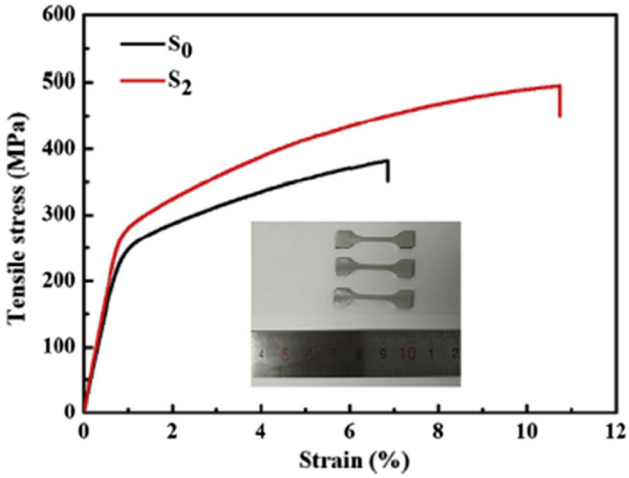

Figure 8 Effect of addition of SiC particle on the tensile stress and strain (S_0 is unreinforced and, S_2 is 2 wt.% nano-SiC-reinforced) [93].

interfacial bonding. Increasing the SiC volume fraction also increases the hardness [89].

The increase in the laser intensity, which depends on the laser power and scanning speed, increases the hardness [90]. Increasing the laser intensity also strengthens the interfacial bonding by increasing the chemical reactions between the SiC particles and the Al matrix. However, increasing the laser intensity too much can increase the keyhole porosity as discussed in the densification behavior section and these keyhole porosities may cause a decrease in the hardness [97]. However, in general, increasing laser intensity (increasing laser power or decreasing scanning speed) tends to increase in the hardness [88].

The addition of SiC particles increases the tensile strength and strain as shown in Fig. 8 [93]. Dislocations at the cell boundaries prevent dislocation motions and allow more dislocations to be stored [93]. Si and Mg_2Si particles formed at the cell boundaries by interfacial reactions prevent dislocation motions through the Orowan mechanism [102], thus contributing to the further development of mechanical properties [97]. Nanosized hard Al_4C_3 precipitates also increase tensile properties. Grain refinement is another factor that increases strength and strain simultaneously. However, it has also been observed that SiC reinforcement may have a negative effect on the tensile stress. The decrease in tensile strength is attributed to the low density as a result of the pores in the composite with the addition of SiC. It has been emphasized that the pores in the structure can lead to nucleation of microcracks, which may cause premature fracture [88].

When the fractographs of SiC-reinforced composites were examined, it was observed that the fracture mode was brittle fracture as shown in Fig. 9 [91]. The bonding between adjacent tracks and adjacent layers are metallurgically weak zones [103]; thus, the fracture started in adjacent tracks and adjacent layers. Under tensile loading, cracks start at the overlapping layer boundaries in parts produced by the LPBF method, which leads to premature fracture [104, 105]. The high laser energy density contributes to high stress and strain by increasing the bonding between adjacent tracks and adjacent layers [97]. Moreover, reducing the SiC particle size in the matrix provides an increase in the geometrically necessary dislocation density, which increases the strength by impeding dislocation motions [91]. As the particle size decreases, the load transfer of the matrix to the reinforcing increases, which leads to the initiation of deformation under higher load [106].

From the literature survey, it was found that SiC particles are applicable reinforcement to increase the mechanical properties of the Al-based composites produced by LPBF method. The homogeneous dispersion of the SiC reinforcement and the matrix material significantly affects the microstructure, porosity and mechanical properties. SiC fraction, size, morphology and LPBF process parameters appear as other factors affecting part quality. The summary of the literature review is shown in Table 3.

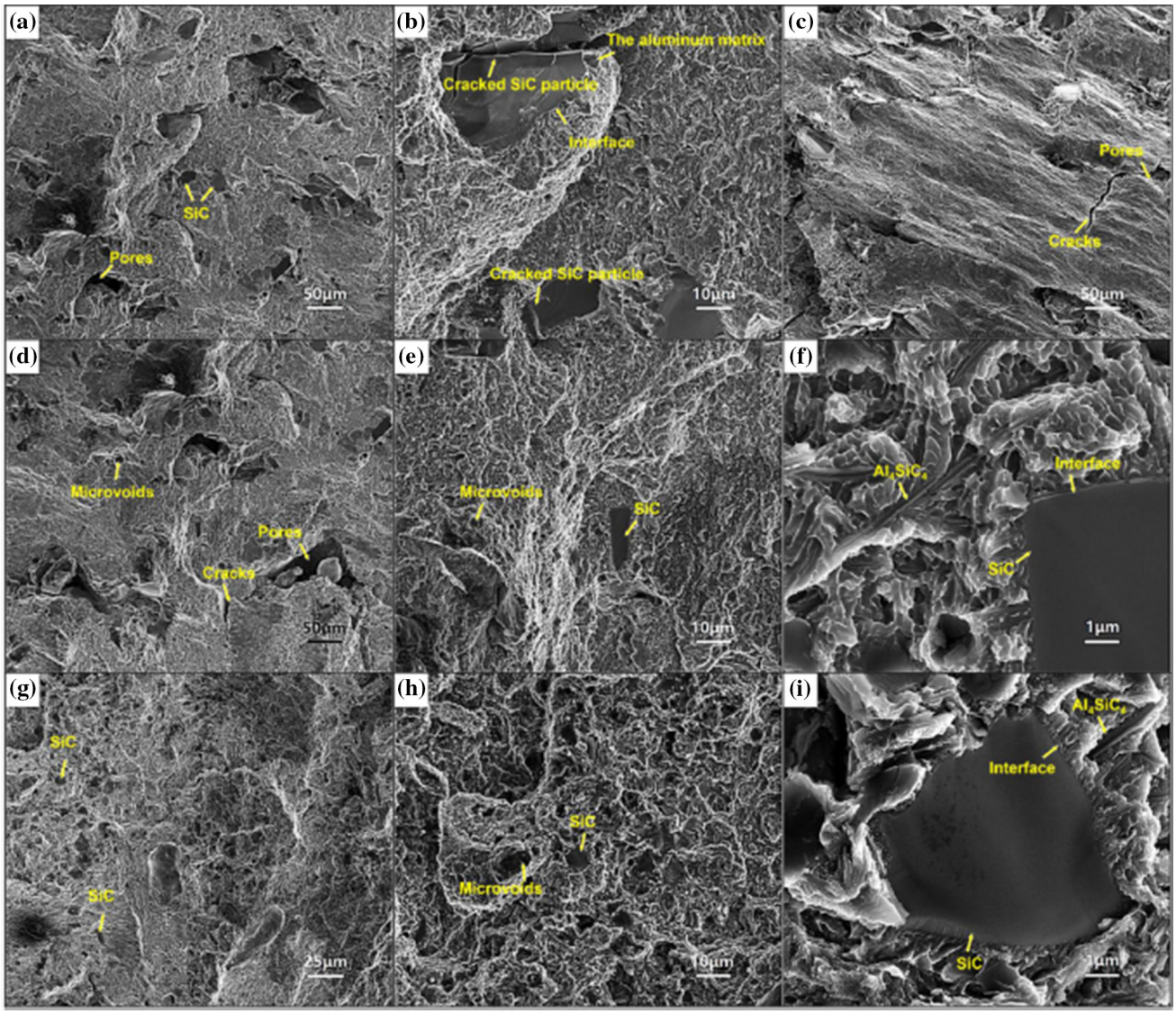

Figure 9 Fracture surface of LPBFed SiC-reinforced composites with different particle size: **a**–**c** 300 mesh, **d**–**f** 600 mesh and, **g**–**i** 1200 mesh [91].

Reinforced by TiC particles

TiC ceramic particles are frequently used as a reinforcement elements in Al-based MMCs due to their superior properties such as high elastic modulus, high hardness and good wettability [107]. The basic physical properties of TiC are listed in Table 4 [108]. Studies show that TiC particles are mostly nanosized, because the refined reinforcing particles effectively improve the mechanical properties of the composite [109, 110]. Composites produced with nanoparticles are known as nanocomposites, and studies on the production of nanocomposites with LPBF have increased significantly in recent years.

Microstructural characterization

The reinforcement size, shape, fraction and LPBF process parameters have different effects on the microstructure in Al-based MMCs with nano- and microsized TiC. It was determined that the microstructure became coarser with the increase in the fraction of reinforcing particles [111]. The addition of TiC to the Al matrix tended to increase the viscosity of the melt, making the flow of the melt difficult and reducing its rheological performance [112]. In addition, the high laser energy intensity caused the formation of high temperature gradients in the molten pool. The temperature gradients in the

Table 3 Summary of the literature review for SiC-reinforced Al-based matrix produced by LPBF

LPBF process parameters				Matrix	SiC fraction	SiC size	Relative density[a]	Hardness[a]	Tensile strength[a]	Elongation[a]	References
Laser power (W)	Scan speed (mm/s)	Layer thickness (μm)	Hatch space (mm)								
300–400	300	50	0.05	Pure Al	20 wt.%	30 μm	91.1%	191 $HV_{0.1}$			[154]
350	1200	40	0.19	AlSi7Mg	2 wt.%	40 nm		2.11 ± 0.2 GPa (194.8–235.5 HV)	502 MPa	10.6 ± 1.06%	[93]
500	1200	40	0.12	AlSi19Mg	15 wt.%	10-23-48 μm	98.9%	316.1 $HV_{0.2}$	763.9 MPa (compressive)	7%	[91]
100	100	30	0.05	AlSi10Mg	20 wt.%	5-15-50 μm	97.2%	218.5 $HV_{0.1}$			[92]
200	375–1750	50		Al12Si	10 vol.%	25 μm	97.4%				[87]
340–490	600–2100	40	0.06–0.18	AlSi10Mg	15 wt.%	46.1 μm	97.7%	217.4 $HV_{0.2}$	341.9 MPa	3.2%	[88]
70–190	50–600	50	0.05	AlSi10Mg	20 wt.%	7 μm	96.1%	214 $HV_{0.1}$			[90]
350	2500	50	0.05	AlSi10Mg	8.5 vol.%	3.5 μm		2.27 GPa (231.5 HV)			[155]
120–240	250	30	0.06	AlSi10Mg	2 vol.%	40 nm	98.7%	135.6 ± 3.5 $HV_{0.1}$	450 ± 30 MPa	4.9 ± 0.78%	[97]
240–320	500–1800	30	0.08–0.16	AlSi10Mg	10 wt.%	10 μm		208.5 $HV_{0.1}$	450 MPa	1.2%	[159]
300–400		50		Al	15 wt.%	30 μm	92.2%	152.6 $HV_{0.1}$			[160]

[a]The maximum values are considered

Table 4 Basic physical properties of TiC [108]

Elastic modulus	Flexural strength	Hardness	Poisson's ratio	Density
410–510 GPa	240–390 MPa	28–35 GPa (2855–3569 HV)	0.191	4.91 g/cm^3

molten pool increase the surface tension gradients and resultant Marangoni convection [111]. Therefore, the undercooling degree of molten pool decreases and causes a low nucleation rate and hence coarsens the microstructure [113].

It was observed that the grain size decreased with the addition of TiC [19]. The thermal conductivities of AlSi10Mg and TiC particles are 103 W/m/K and 330 W/m/K, respectively [114, 115]. With the addition of TiC particles, the thermal conductivity of the composite increases, leading to a high solidification rate and thus refined grains. In addition to thermal conductivity, the laser absorptivity of the pure AlSi10Mg powder and TiC particles is 0.09 and 0.82, respectively [116, 117]. The increase in laser absorptivity increases the temperature gradients in the molten pool, resulting in a more homogenous distribution of TiC particles [118–120].

Besides reinforcing particle properties, LPBF process parameters have a significant impact on the microstructure. In order to examine the effects of laser power and scanning speed on the microstructure, microstructure characterizations were made by producing parts with different laser energy densities (η), which was defined by [121]:

$$n = \frac{P}{v} \tag{3}$$

where P is the laser power and v is the scanning speed.

Figure 10 shows the microstructures of TiC/AlSi10Mg nanocomposite with different η [122]. At the low η it was observed that, TiC particles agglomerates in the matrix. Increasing the η provided a more homogeneous distribution of TiC particles and almost no agglomeration [123]. In addition, the average size of TiC particles increased with the increase of η. Especially at very high η, the TiC particles lost their favorable initial morphology [90].

The melt pool temperature, which improves significantly when high laser energy density is applied, leads to a decrease in viscosity and consequently intensification of the Marangoni flow [124]. With the decrease in viscosity, the rearrangement rate of nanosized TiC particles increases, thus avoiding

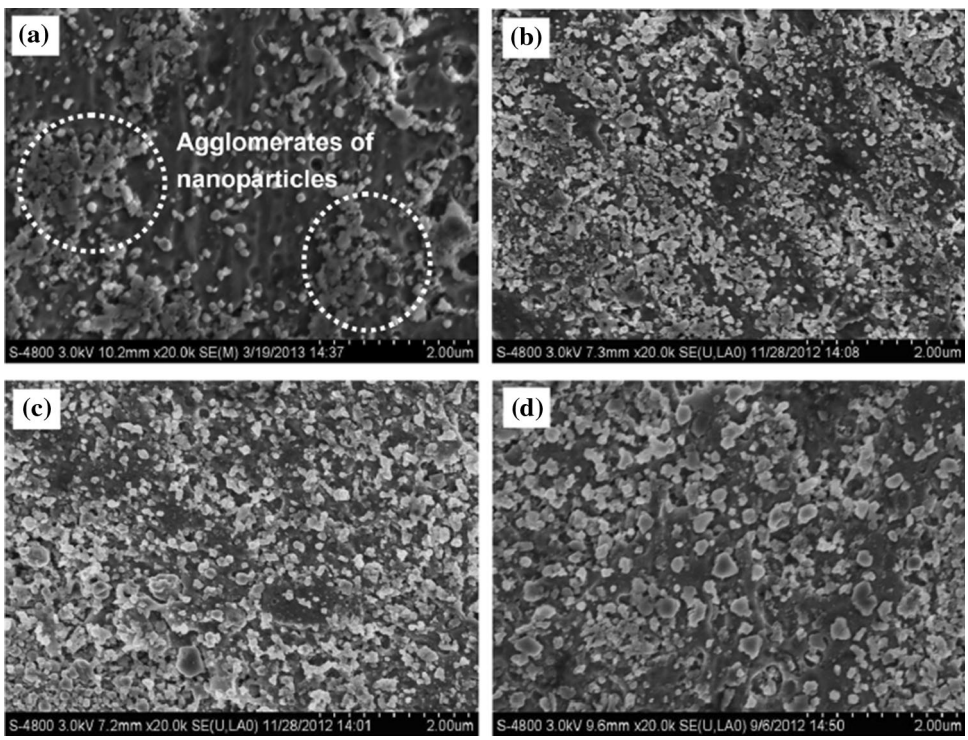

Figure 10 Microstructure of LPBFed TiC/AlSi10Mg nanocomposites at various laser energy density: **a** 250 J/m, **b** 500 J/m, **c** 700 J/m and **d** 1000 J/m [122].

agglomeration. At low laser energy density, the solidification rate of the molten pool increases. Grain growth of TiC particles is inhibited by the rapid solidification rate and the initial morphology is preserved [122, 125].

Densification behavior

In the LPBF method, the densification behavior is related to the melt pool viscosity, wettability and liquid/solid rheological properties. The dynamic viscosity of melt pool containing Al–Si–Mg liquid can be defined by [43]:

$$\mu = \mu_0 \left(1 - \frac{1-\varphi_1}{\varphi_{\mathrm{m}}}\right) \tag{4}$$

where μ_0 is the base viscosity that includes temperature terms, φ_1 is the volume fraction of liquid phase and φ_m is a critical volume fraction of solids above which the mixture has essentially infinite viscosity.

The densification level is controlled by the base viscosity, which is directly related to the temperature [126]. The base viscosity decreases with increasing temperature and leads to better wettability, thereby improving the densification level. At low laser energy density, viscosity increases due to the low temperature in the molten pool. The high viscosity results in poor wettability characteristic and consequently low densification level [127, 128]. Meanwhile, the addition of TiC increases the densification level due to the increase in laser absorption, while it decreases the densification level due to its tendency to increase the viscosity. To summarize, limited wettability and high melt viscosity are the main factors to determine the densification behavior of TiC-reinforced composites.

LPBF process parameters affecting the melt pool temperature, especially laser power and scanning speed, have significant effects on the densification behavior. At low laser energy density, irregular-shaped interlayer porosities are formed in the composite structure. With the increase in the laser energy density, it is revealed that the porosities in the composite get smaller and almost no porosity occurs at a certain level (Fig. 11) [122]. However, it has also been reported that there are decreases in the density of the composite at excessive laser energy densities. Excessive laser energy density may cause the turbulence in the molten pool or evaporation, resulting in a decrease in density [119].

Besides the process parameters, HIP as a post-process also has important effects on the densification characteristics. With the HIP process, it was determined that the porosity of pure AlSi10Mg decreased

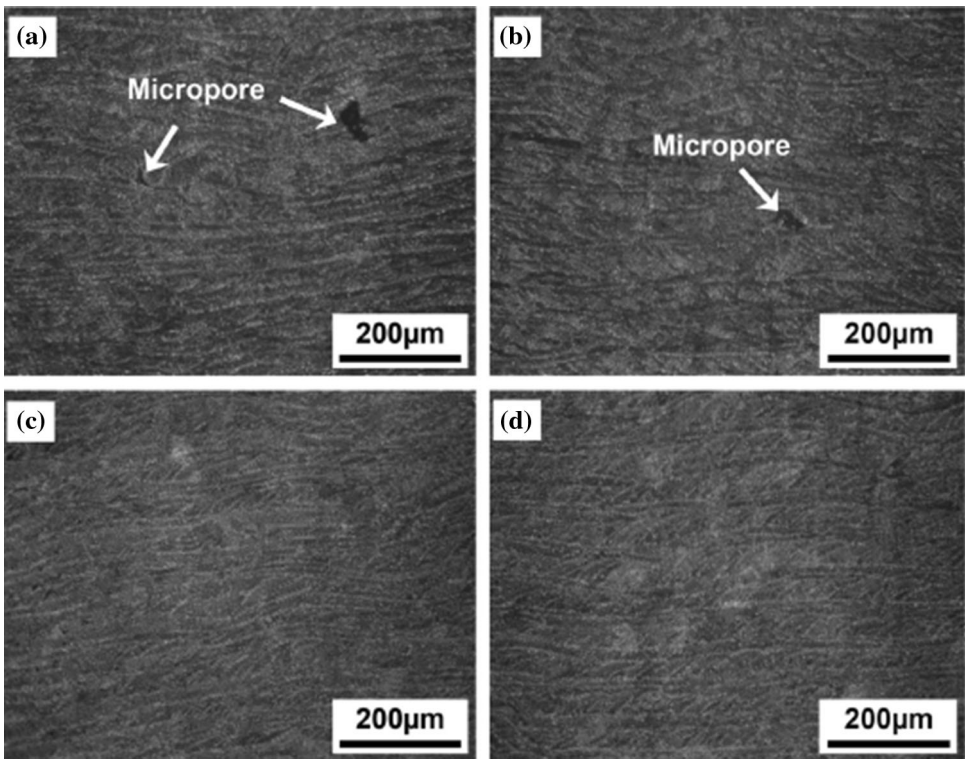

Figure 11 Microstructures of SLM-processed TiC/AlSi10Mg nanocomposites at different laser energy density, **a** 250 J/m, **b** 500 J/m, **c** 700 J/m and **d** 1000 J/m [122].

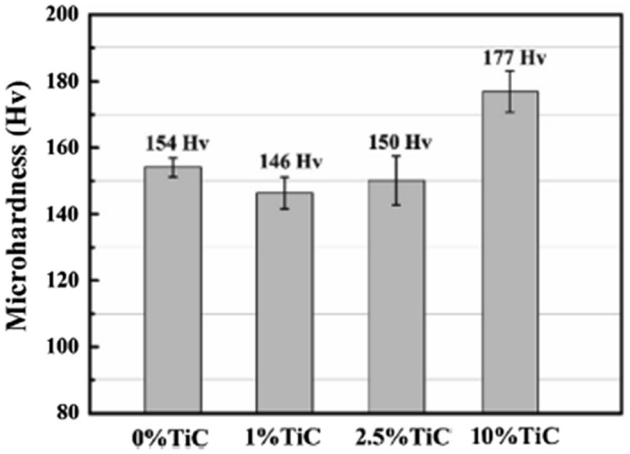

Figure 12 Effect of different TiC contents on microhardness of TiC/Al-15Si composite [111].

from 1.32% to 0.38%, and the porosity of TiC-reinforced AlSi10Mg composite decreased from 1.82% to 0.42%.

Hardness and tensile properties

The hardness of the composites increases with the addition of TiC particles as a reinforcement. The hardness of TiC/AlSi10Mg nanocomposite can reach 185 HV and this value is 21% higher than the hardness of unreinforced AlSi10Mg [5, 129]. In a study using Al-15Si as the matrix material, it was determined that the hardness decreased slightly with the addition of 1% and 2.5% TiC, while the hardness increased with the addition of 10% TiC (Fig. 12) [111]. This increase can be attributed to the presence of high fraction of hard TiC particles and primary Si precipitation. TiC particle size is another factor that affects hardness. It was observed that the hardness of the composite increased with the decrease in the TiC particle size [119]. The high hardness largely depends on the uniform and homogeneous distribution of TiC particles in the matrix. With the reduction in the TiC particle size, TiC particles in the powder mixture are mixed more homogeneously with the matrix powders, leading to the production of parts at almost full density, a more uniform TiC distribution and therefore an increase in hardness. In addition, uniformly distributed TiC particles improve the strength of the interfacial bonding and thus contribute to the increase in hardness.

The variation in microhardness at different laser energy densities is presented in Fig. 13 [122]. The increase in laser energy density contributes to the improvement of hardness. The increase in hardness with the increase in the laser energy density can be attributed to the uniform distribution of TiC particles and the improvement of part density [128]. However, further increase in laser energy density (> 800 J/m) has a negative effect on hardness [112]. The hardness decreases as a result of grain growth, more defects in microstructure and reduction in the density at excessive laser energy density.

With the addition of TiC, the tensile strength of composite increased from 400 to 482 MPa, while the elongation was consistent with the unreinforced part [129]. The increase in tensile strength without a decrease in ductility can be attributed to the increase in dislocation density at reinforcement/matrix interfaces by causing dislocation pileup of TiC particles [130, 131]. In addition, TiC particles act as a barrier against dislocation movements, increasing the tensile strength. The weight/volume ratio of TiC particles in the composite also has important influences on the tensile properties. It was determined that both tensile stress and ductility increased with the addition of 1% and 2.5% TiC to the Al-15Si matrix, while both values decreased with the addition of 10% TiC. The reason for the reduction in the tensile stress at the addition of 10% TiC is the rapid precipitation of Si atoms trapped in the Al matrix onto the existing eutectic network Si [111]. In the case of using 1 μm TiC particles, tensile stress increased from 410 to 470 MPa, while elongation decreased from 8.9% to 4%.

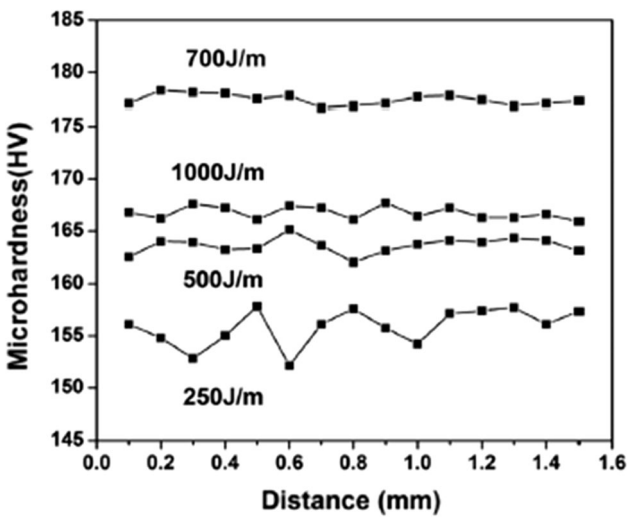

Figure 13 Variation in microhardness at different laser energy densities [122].

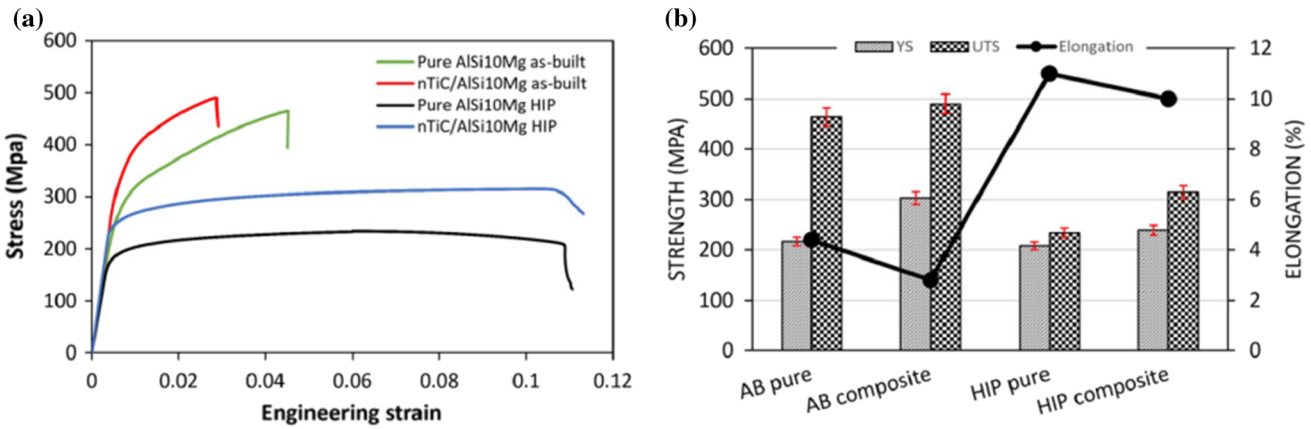

Figure 14 Tensile properties of pure AlSi10Mg and nTiC/AlSi10Mg before and after HIP process, **a** engineering stress–strain curves, **b** comparison of UTS, YS and elongation [19].

However, when 30 μm TiC particles were used, tensile stress and elongation were simultaneously reduced compared to the unreinforced material [119]. The reduction in tensile properties can be attributed to the balling effect, which tends to break up into several spherical agglomerates to reach equilibrium due to the high viscosity of the liquid in the molten pool [132].

Compared to the unreinforced part, the tensile stress of the TiC-reinforced composite increased from 400 to 452 MPa at an energy density of 160 J/mm and increased to 486 MPa at an energy density of 240 J/mm. Ductility values decreased from 10.7 to 9.8% at 160 J/mm and increased to 10.9% at 240 J/mm. The homogeneous distribution of TiC particles at an energy density of 240 J/mm and the ring structures formed in the microstructure increased both tensile stress and ductility [125]. The increase in part density with the increase in the laser energy density is another reason for the increase in tensile properties.

In Fig. 14, the tensile properties of TiC-reinforced and unreinforced parts before and after the HIP process are presented [19]. It is seen that the tensile stress increases and elongation decreases with the addition of TiC. The reason for the decrease in elongation was attributed to the increase in porosity and dislocation density with the addition of TiC [133]. After the HIP process, the tensile strength of the reinforced and unreinforced parts decreased, but the elongation increased drastically. The work hardening effect on reinforced and unreinforced parts has been vanished by the HIP process, and the material has been homogenized. In addition, the elimination of dislocation walls is another reason for the increase in ductility [19]. To sum up, the HIP process is an important post-process that increases the ductility of reinforced and unreinforced parts produced with LPBF.

From the literature survey, it was found that TiC particles are another applicable reinforcement to increase the mechanical properties of the Al-based composites produced by LPBF method. Homogeneous mixture of TiC reinforcement and matrix material, TiC fraction and size, as well as LPBF process parameters are significant factors affecting part quality. As a post-process, HIP has significant effects on the mechanical properties of the composite. With the HIP application, the internal pores have decreased, and thus, the ductility has increased significantly. The summary of the literature review is shown in Table 5.

Reinforced other ceramic particles

In addition to SiC and TiC reinforcements, research works are conducted in which TiB_2, TiN and Al_2O_3 ceramics are used as reinforcement elements. These ceramics are used extensively in Al-based composites due to their superior mechanical properties. In Fig. 15, SEM images of composite feedstocks prepared with micro- and nanosized TiB_2 reinforcement [134] and microsized Al_2O_3 reinforcement are presented [135]. TiB_2/AlSi10Mg feedstock was prepared with ball milling in 48 h without any grinding medium, and Al_2O_3/AlSi10Mg feedstock was prepared in 10:1 ball-to-powder weight ratio with 70 rpm rotation speed in 4 h. It was determined that dispersion state

Table 5 Summary of the literature review for TiC-reinforced Al-based matrix produced by LPBF

LPBF process parameters				Matrix	TiC fraction	TiC size	Relative density[a]	Hardness[a]	Tensile strength[a]	Elongation[a]	References
Laser power (W)	Scan speed (mm/s)	Layer thickness (μm)	Hatch space (mm)								
360	650	20	0.06	Al-15Si	1–2.5–10 wt.%	6.7 μm		177 HV	578 MPa	7.86%	[111]
300	1000–1800	30	0.1	AlSi10Mg	15 wt.%	1–30 μm	> 98%	169 $HV_{0.1}$	470 MPa	3.74 ± 0.5%	[119]
110	100–350	50	0.05	AlSi10Mg	5 wt.%	50 nm	> 98%	181.2 $HV_{0.2}$			[112]
100	100–400	50	0.05	AlSi10Mg	5 wt.%	50 nm	> 98%	177.6 $HV_{0.2}$			[122]
80–140	100–500	30	0.05	AlSi10Mg	4 wt.%	50 nm	> 98.5%	184.7 $HV_{0.1}$			[128]
100	150	50	0.05	AlSi10Mg	5 wt.%	1.5 μm		185 $HV_{0.1}$	482 MPa	10.8%	[129]
80–140	200	50	0.05	AlSi10Mg	3 wt.%	50 nm		188.3 $HV_{0.1}$	486 MPa	10.9%	[125]
250	400	25	0.045	AlSi10Mg	3 wt.%	80 nm	98.18% 99.58%[b]		302 MPa 239.7 MPa[b]	2.8% > 10%[b]	[19]

[a]The maximum values are considered

[b]These data are obtained after HIP

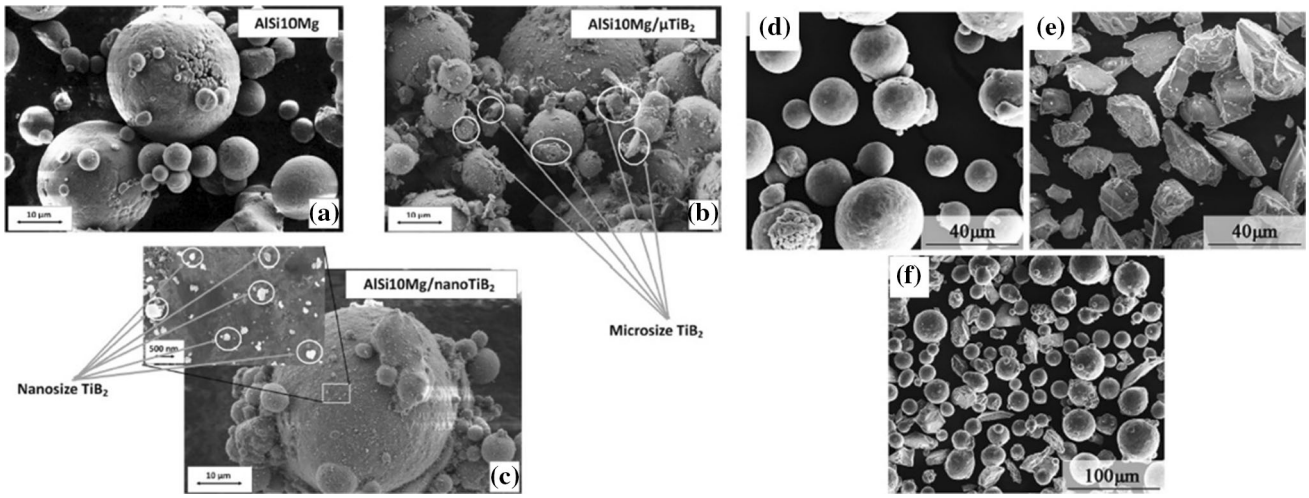

Figure 15 Scanning electron micrographs of powders: **a** AlSi10Mg, **b** 10 wt.% TiB_2(μm)/AlSi10Mg, **c** 1 wt.% TiB_2(nm)/AlSi10Mg [134] and **d** AlSi10Mg, **e** Al_2O_3, **f** Al_2O_3/AlSi10Mg [135].

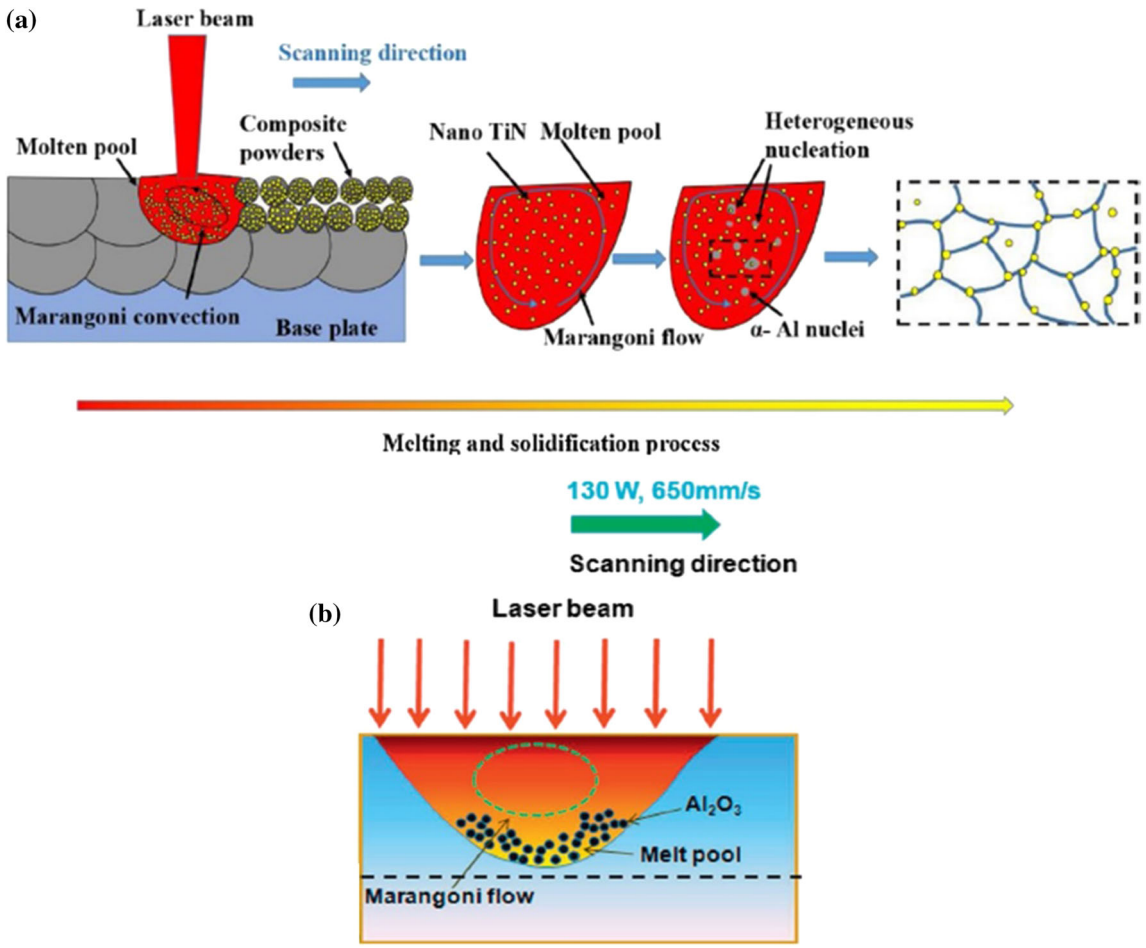

Figure 16 **a** Schematic representation of behaviors of Al_2O_3 reinforcing particles in melt pools [136], **b** schematic representation of the microstructural development for the TiN/AlSi10Mg composites during LPBF process [138].

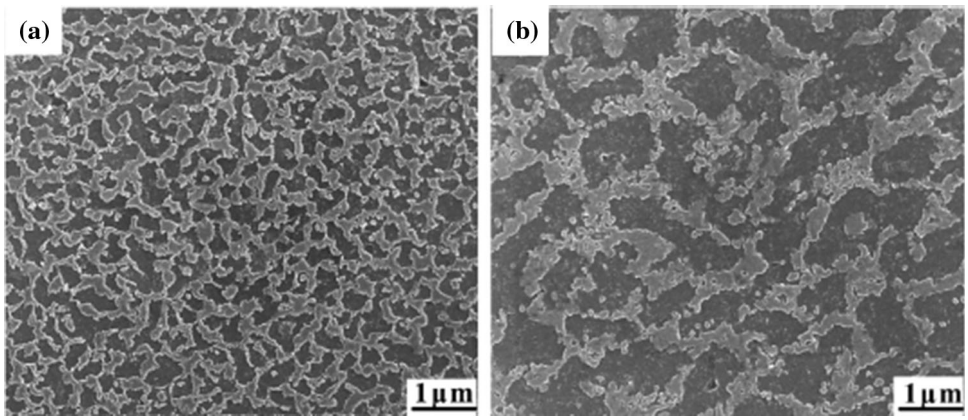

Figure 17 SEM images of: **a** TiN/AlSi10Mg nanocomposite and **b** AlSi10Mg microstructure [139].

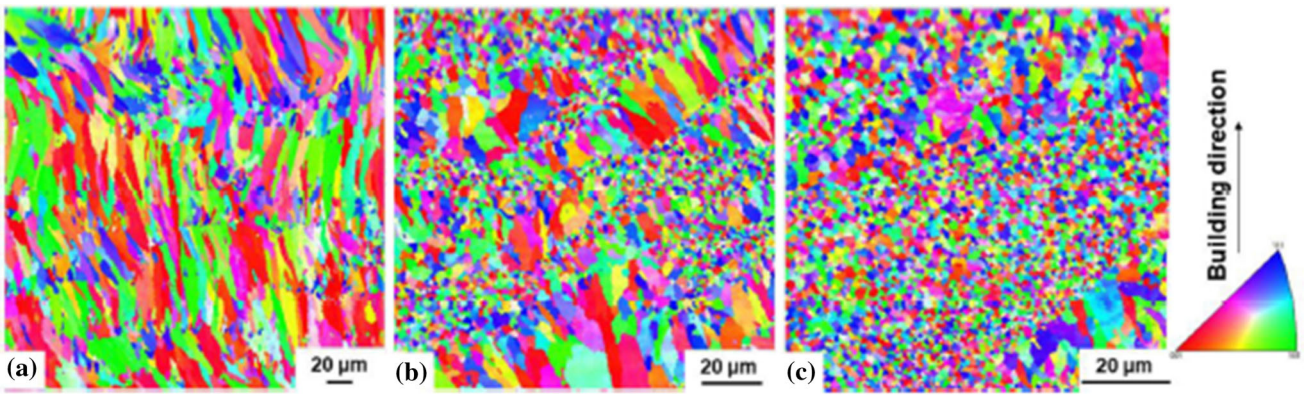

Figure 18 EBSD inverse pole figure maps of TiB_2/AlSi10Mg composites with different reinforcement fractions: **a** 1 wt.%, **b** 2 wt.% and **c** 5 wt.% TiB_2 [141].

and sphericities of the mixed powders do not change markedly in both composite feedstock.

Microstructural characterization

In Fig. 16 a, the microstructural development of TiN/AlSi10Mg composite is shown schematically [136]. In the LPBF process, Marangoni flow is formed by a high temperature gradient from the edge to the center of the molten pool [71]. Due to the high melting temperature, the unmelted ceramic reinforcements flow and rearrange with the Marangoni flow. As a result, most of the reinforcing elements are pushed and distributed along the grain boundaries during the solidification process. Only limited number of particles act as heterogeneous nucleation sites [137]. In Fig. 16 b, the behavior of Al_2O_3 particles in the molten pool is shown schematically [138]. The distribution state of the Al_2O_3 particles in the molten pool mainly depends on the interaction between the reinforcement particles and the advancing solid–liquid interface.

The microstructures of TiN/AlSi10Mg composite and AlSi10Mg are presented in Fig. 17 [139]. It is seen that the grain size of the composite is more refined than the unreinforced AlSi10Mg part. Since the interaction between the laser beam and the powders is extremely short in the LPBF process, the unmelted ceramic reinforcements and the molten matrix are simultaneously present in the molten pool. Solid-state reinforcing elements act as heterogeneous nucleation sites, improving the nucleation rate and therefore causing grain refinement [140]. Gao et al. [71] determined that the grain size depends on the laser process parameters. They stated that the grain size increased from 0.284 to 0.388 µm as a result of the increase in thermal gradients and cooling rate with the decrease in the scanning speed from 600 to 200 mm/s.

In Fig. 18, EBSD inverse pole figures of composites produced at different TiB_2 reinforcement content are

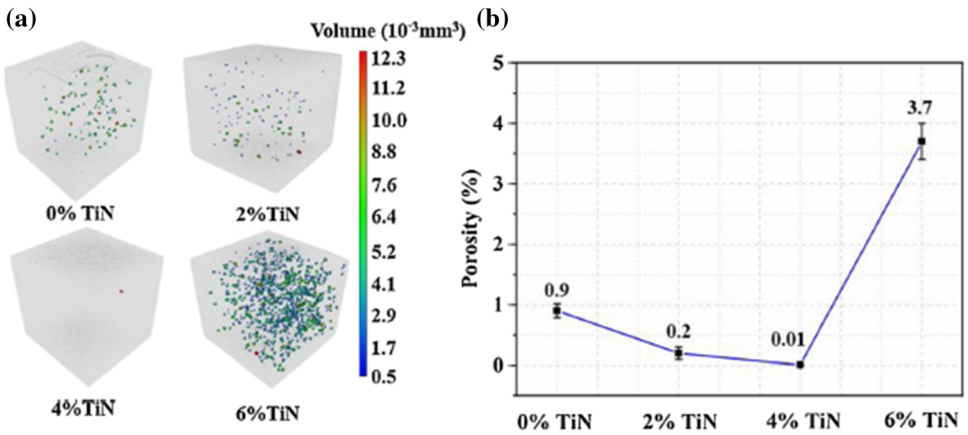

Figure 19 **a** Micro-CT images of porosity distribution of different reinforcement weight ratios TiN/AlSi10Mg composites, **b** the porosity as a function of TiN content [138].

presented [141]. The grain size of the composite became more refined as the reinforcement content increased. TiB_2 particles act as grain growth inhibitor, thus limiting the growth of grains along the heat flux direction, similar to other ceramic particles [142]. The grain sizes of the composites produced with 1% and 5% reinforcement content were measured as 6.32 ± 0.07 µm and 1.55 ± 0.14 µm, respectively. In summary, the fact that composites produced with ceramic reinforcements have more refined grains is

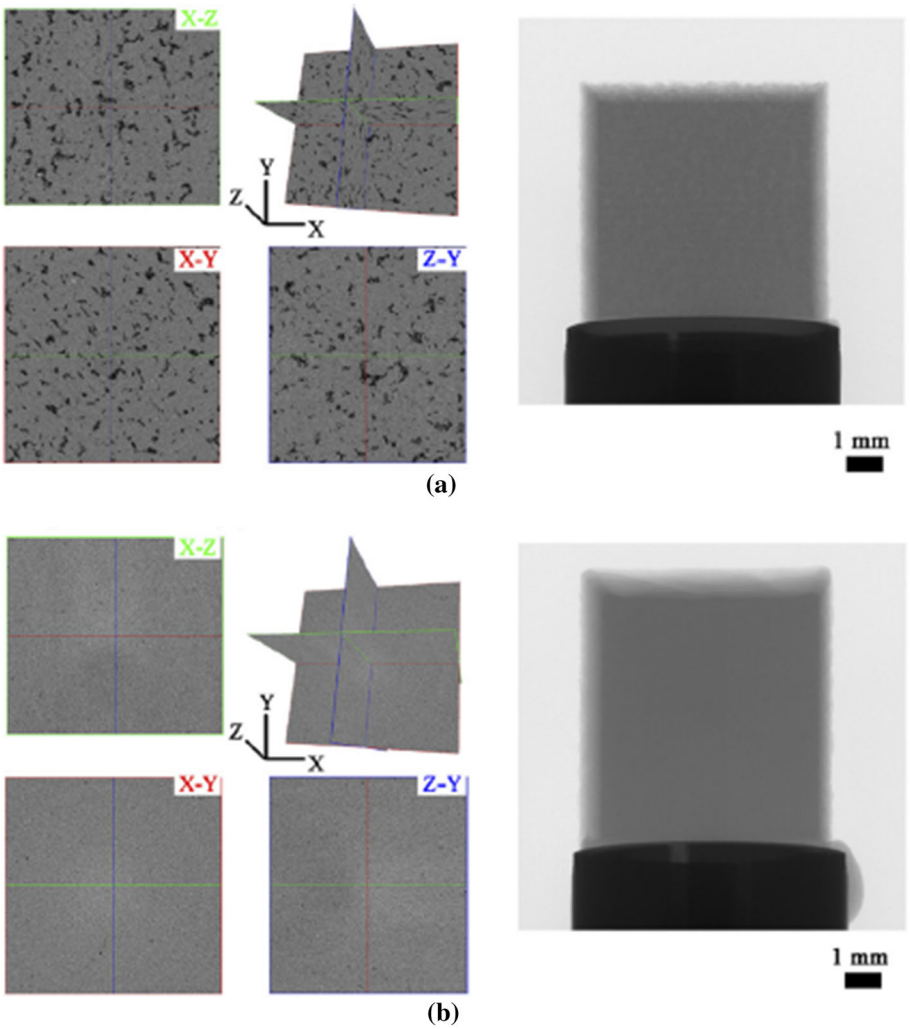

Figure 20 Micro-CT images of porosity distribution of 2 wt.% Al_2O_3/AlSi10Mg composite at different volumetric energy densities: **a** 23.33 J/mm^3, **b** 109.38 J/mm^3 [144].

attributed to a combination of increased nucleation sites, limitations on grain growth and rapid solidification rate during LPBF.

Densification behavior

The densification behavior of ceramic-reinforced composites produced with LPBF is significantly affected by the physical and chemical properties of the feedstock powders as well as the LPBF process parameters. Micro-CT images of TiN/AlSi10Mg composite produced at different reinforcement weight ratios and porosity values as a function of TiN content are presented in Fig. 19 [138]. It is seen that the porosity decreases with the increase in the reinforcement content from 0 to 4%, but the porosity increases with its further increase. With the addition of TiN as a reinforcing element, the reduction in the laser reflectivity increases the melt pool temperature and decreases the melt viscosity [139]. In addition, nanosized reinforcements provide lower melt pool viscosity than microsized reinforcements [143]. With the decrease in viscosity, sufficient melt flow is ensured, and the melt fills the voids more easily, thus increasing the composite density. Moreover, the higher temperature in the molten pool provides better wettability [144]. In this way, a stronger bonding is formed between the reinforcement and the matrix, and the formation of pores and cracks at the interface is reduced.

However, if the reinforcement content exceeds a certain threshold, it negatively affects the composite density. The use of a high content of reinforcement makes it difficult to prepare a homogeneous feedstock. Moreover, reinforcement particles, especially at the nanoscale, tend to agglomerate due to their high surface energy and specific surface area. The agglomeration of the unmelted reinforcements in the molten pool increase the porosity [138]. Solid-state reinforcements in the molten pool also increase the melt viscosity, causing the formation of more defects and pores.

Micro-CT images of Al2O3/AlSi10Mg composite produced at different volumetric energy densities are presented in Fig. 20 [144]. In general, it has been stated that increasing the laser power and decreasing the scanning speed increase the composite density due to elevating the melt pool temperature and decreasing the melt viscosity. At low laser power and high scanning speeds, high viscosity causes poor wettability, resulting in the formation of pores and defects in the molten pool [141]. Research works in the literature have suggested different optimum process parameters for the production of nearly fully dense composites with different reinforcement. Xi et al. [145] produced 1 wt%, 2 wt% and 5 wt% composites with TiB_2 reinforcement and stated that the maximum relative density was obtained at 1800 mm/s scanning speed. Li et al. [146] investigated the densities of TiB_2/AlSi10Mg composite produced in different parameter sets and obtained higher relative density at 400 W laser power and 2000 mm/s scanning speed. Gao et al. [71] stated that the relative density decreased with increasing scanning speed for nano-TiN/AlSi1OMg composite, and the highest relative density was obtained at the

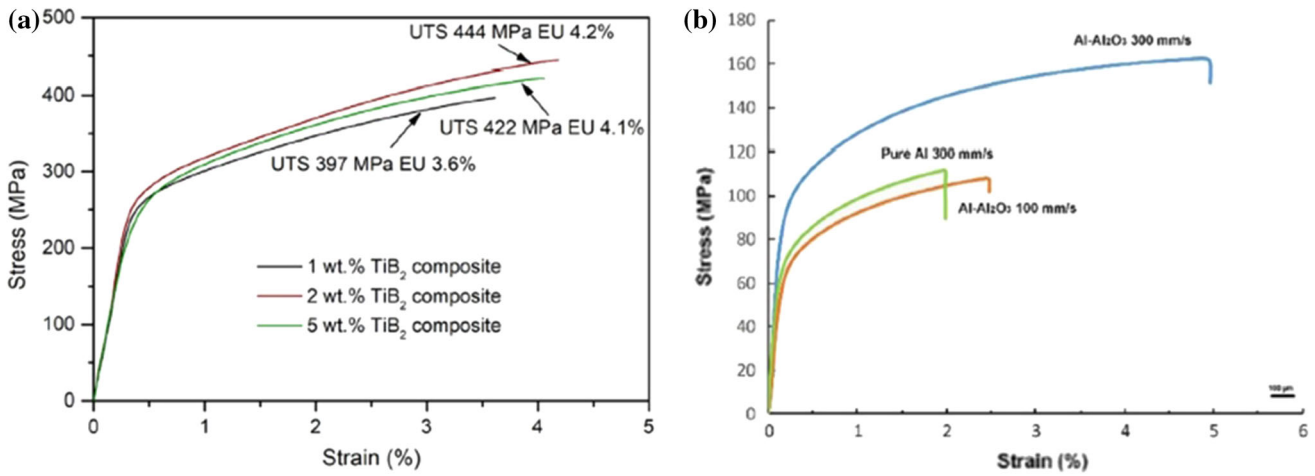

Figure 21 Tensile stress–strain curves of: **a** TiB_2/AlSi10Mg composite different reinforcement fractions [141], **b** pure Al and Al_2O_3/Al composites [70].

scanning speed of 200 mm/s. Han et al. [70] determined that the optimum laser energy density for Al/Al_2O_3 composite was 317.5 J/mm^3, and the relative density decreased above and below this critical threshold. As a result, it is revealed that the LPBF process parameters have significant effects on the composite density, and different process parameters should be used depending on the reinforcement for the production of nearly fully dense composites.

Hardness and tensile properties

In Fig. 21 (a), tensile stress–strain curves of TiB_2/AlSi10Mg composite produced with different reinforcement contents are presented [141] and Fig. 21 b shows the tensile stress–strain curves of pure Al and composite samples under different scanning speed [70]. With the use of ceramic particles as reinforcement, the hardness and tensile properties of composites improve. The yield strengths of the pure Al-12Si alloy and the reinforced with 2% TiB_2 composite were measured as 211 ± 4 and 225 ± 4 MPa, respectively [147]. The hardness and tensile properties of the ceramic-reinforced composite materials are largely dependent on the reinforcement size and content, homogeneous dispersion of the reinforcements and the matrix and interfacial bonding between matrix and reinforcement.

There are different strengthening mechanisms in ceramic-reinforced composites, including grain refinement effect, dislocation density strengthening, Orowan strengthening and load-bearing strengthening through strong interfacial bonding [73, 94, 148]. However, especially if the reinforcement content exceeds a certain threshold, it can cause negative effects on the hardness and tensile properties, since it causes the formation of pores by increasing the melt viscosity. The ultimate tensile stresses of the composites produced with 2% and 5% TiB_2 content were determined as 444 MPa and 422 MPa, respectively [141] and the yield strength of the composites produced with 2%, 4% and 6% nano-TiN content was measured as 295.9 ± 4.6, 315.4 ± 5.2 and 261.6 ± 3.5 MPa, respectively [138].

As a result of the literature review, it has been revealed that TiB_2, TiN and Al_2O_3 ceramic reinforcements can be used in the production of nearly fully dense composites by LPBF method. In order for the composite quality to be at the desired values, it is necessary to mix the reinforcement and matrix powders homogeneously, and to use the appropriate reinforcement content and laser process parameters. Too long or too short the interaction of the laser beam and the powder negatively affects the rheology of the molten pool and causes the formation of pores in the molten pool. The summary of the literature review for the TiB_2, TiN and Al_2O_3 reinforcements is shown in Table 6.

Conclusions and future research

This study presents a comprehensive review of the production of ceramic particle-reinforced Al-based composites by LPBF method. The manufactured composites were characterized in terms of microstructure, densification behavior and mechanical properties (hardness and tensile properties) which have the most significant effects in the widespread application of MMCs. The effects of reinforcing particle properties such as type, morphology, size and content as well as LPBF process parameters on the composite properties were evaluated.

From the literature survey, it is revealed that the LPBF is a promising method for producing high-quality, low-cost, repeatable and nearly fully dense ceramic particle-reinforced Al-based MMCs. In addition to the LPBF method, composite production processes are investigated by using various reinforcement elements and matrix materials in different AM techniques such as direct ink writing (DIW) [149], stereolithography (SLA) [150] and digital light processing (DLP) [151]. Particularly, carbon fiber-reinforced ceramic and metal matrix composites are intensively studied [152, 153]. These studies show that these AM techniques are promising methods for producing complex-shaped and high-quality ceramic and metal matrix composites at a lower cost than conventional methods.

The flexibility that LPBF offers in the use of different feedstocks indicates that it would be increasingly used in MMC production. However, it is necessary to pay attention to numerous issues in composite production in LPBF, which is a complex process. The selection of reinforcement is the primary issue as it will affect the chemical reactions and the evolution of the internal defects. The chemical reactions that occur between the matrix and the reinforcement cause the formation of new phases at the interface. In order to evaluate the microstructure and

Table 6 Summary of the literature review for other ceramic particle-reinforced Al-based matrix produced by LPBF

Reinforcement	LPBF process parameters				Matrix	Reinforcement fraction	Reinforcement size	Relative density[a]	Hardness[a]	Tensile strength[a]	Elongation[a]	References
	Laser power (W)	Scan speed (mm/s)	Layer thickness (μm)	Hatch space (mm)								
TiB_2	320	1655	50	0.11	Al-12Si	2 wt.%	3.5–6 μm	> 98%	142 ± 6.0 $HV_{0.05}$	247 ± 4 MPa (yield)		[161]
	320	1655	50	0.11	Al-12Si	2 wt.%	3.5–6 μm	≈ 99.1%	142 ± 6.0 $HV_{0.05}$	225 ± 4 MPa (yield)		[147]
	350–450	1800	50	0.05	AlSi10Mg	1 wt.%	Submicron	> 99%	126 $HV_{0.2}$			[145]
	450	1600–2600	50	0.05	AlSi10Mg	1-2-5 wt.%		~99.0%	129 $HV_{0.2}$	~444 MPa	~4.2%	[141]
	450	1800–2400	50	0.05	AlSi10Mg	1 wt.%	1.5 μm and submicron	> 99.0%		400 ± 1.4 MPa (submicron)	3.60 ± 0.04%	[143]
	300–400	2000–3200	50		AlSi10Mg	1 wt.%	3–5 μm	> 99.37%	124.4 HV	380 MPa	3.42%	[146]
	160 (μm)	300		0.1	AlSi10Mg	10 wt.% (μm)	2–5 μm		99.2 $HV_{0.1}$			[134]
	180 (nm)					1 wt.% (nm)	60 nm		97.5 $HV_{0.1}$			
TiN	200	1200	30	0.09	AlSi10Mg	4 wt.%	80 nm		156.9 ± 4.9 $HV_{0.1}$	491.2 ± 5.5 MPa	7.53 ± 0.3%	[162]
	100	600	30	0.08	AlSi10Mg	2 wt.%	80 nm		145 $HV_{0.1}$			[139]
	100	200–600	30	0.08	AlSi10Mg	2 wt.%	80 nm	97.6%	145 ± 4.9 HV			[71]
	200	1200	30	0.09	AlSi10Mg	2–4-6 wt.%	80 nm		156.9 ± 4.9 HV	491.8 ± 5.5 MPa	7.5 ± 0.29%	[138]
Al_2O_3	200	100–600	30	0.07–0.1	Al	4 vol.%	50 nm	> 99.49%	≈ 49.48 $HV_{0.1}$	160 MPa	5%	[70]
	200	100–300	20	0.06–0.16	AlSi10Mg	15 wt.%	26.6 μm					[135]
	200	300			Al	4 vol.%	50 nm		48.35 $HV_{0.1}$			[163]
	350	100–1500	50	0.1–0.2	AlSi10Mg	2–5 wt%	270 nm	> 99.6%				[144]
	130	450–750	70		Al	20 wt%	9.04 μm	97.3%	175 $HV_{0.1}$			[136]

[a]The maximum values are considered

internal defects of ceramic-reinforced composite, it is necessary to analyze the chemical reactions and reaction products occurring at the reinforcement–matrix interface. Reinforcements such as TiB_2, CNT and TiC, which react less with the Al matrix, can be considered primarily in the production of Al-based MMCs, as they reduce the formation of undesirable reaction products at the interface. Moreover, different reinforcements exhibit different wetting, solidification and agglomeration behavior during the LPBF process. The agglomeration tendency of nanosized reinforcements have detrimental effects on composite quality. To sum up, find the right reinforcement is the key factor for producing high-quality composites.

One of the other significant issue is to ensure the homogeneous distribution of the particles with a suitable mixing method. Ball milling and regular mixing methods have attracted great attention in recent years due to their practicality, time and cost efficiency, and applicability to a wide variety of materials. However, in both methods, long-term collisions of the powders have negative effects on the powder surface quality. Repeated deformation, fracture and cold welding inevitably degrade the sphericity of the initial powders, which adversely affects the powder flowability and causes a decrease in composite quality. Another undesirable effect of these mixing methods is the inability to reduce the agglomeration effects, especially of nanosized reinforcements. Therefore, the development of a novel and advanced mixing technique which cannot affect the powders initial morphology and surface quality and can provide a homogeneous mixture is considered very important in the production of high-performance composites with LPBF.

A comprehensive understanding of the strengthening mechanisms of composites produced with LPBF would be important in producing parts with high mechanical properties. The addition of ceramic reinforcements increases the mechanical properties of the composites with the grain refinement effect, dislocation density strengthening, Orowan strengthening and load-bearing strengthening through strong interfacial bonding. The most significant factor determining the tensile properties is the bonding between adjacent tracks and adjacent layers. Under tensile loading, cracks start from adjacent tracks and adjacent layers. Better tensile properties can be obtained with stronger bonding. Improving the mechanical properties of composites depends on the elimination of internal defects like porosity and residual stresses. As a post-treatment, HIP and heat treatment would be an effective process to reduce the porosity, release residual stresses and increase the mechanical properties of composites.

When the effects on the microstructure, density and tensile properties of ceramic reinforcements are examined, it is seen that the most important factor is the rheological behavior of the molten pool. Proper selection of reinforcing particle properties and LPBF process parameters which have the effect on rheological behavior of the molten pool is necessary to achieve high-quality composites. As a result of the findings obtained from the literature survey, it is revealed that there is a gap on process optimization, modeling simulation and post-treatment operations such as heat treatments and HIP. In particular, the findings to be obtained by modeling the molten pool can make significant contributions to a better understanding of microstructure formation, solidification behavior and internal defects. By understanding the underlying mechanisms with reliable predictive models, the LPBF process can be optimized.

Declarations

Conflict of interests

The authors declare that they have no conflict of interest.

References

[1] Fiocchi J, Tuissi A, Bassani P, Biffi CA (2017) Low temperature annealing dedicated to AlSi10Mg selective laser melting products. J Alloys Compd 695:3402–3409. https://doi.org/10.1016/j.jallcom.2016.12.019

[2] Zhou C, Hu S, Shi Q et al (2020) Improvement of corrosion resistance of SS316L manufactured by selective laser melting through subcritical annealing. Corros Sci 164:108353. https://doi.org/10.1016/j.corsci.2019.108353

[3] de Damborenea JJ, Arenas MA, Larosa MA et al (2017) Corrosion of Ti6Al4V pins produced by direct metal laser sintering. Appl Surf Sci 393:340–347. https://doi.org/10.1016/j.apsusc.2016.10.031

[4] Liu YJ, Liu Z, Jiang Y et al (2018) Gradient in microstructure and mechanical property of selective laser melted AlSi10Mg. J Alloys Compd 735:1414–1421. https://doi.org/10.1016/j.jallcom.2017.11.020

[5] Buchbinder D, Schleifenbaum H, Heidrich S et al (2011) High power Selective laser melting (HP SLM) of aluminum parts. Phys Procedia 12:271–278. https://doi.org/10.1016/j.phpro.2011.03.035

[6] Murr LE, Gaytan SM, Ramirez DA et al (2012) Metal fabrication by additive manufacturing using laser and electron beam melting technologies. J Mater Sci Technol 28:1–14. https://doi.org/10.1016/S1005-0302(12)60016-4

[7] DebRoy T, Wei HL, Zuback JS et al (2018) Additive manufacturing of metallic components—Process, structure and properties. Prog Mater Sci 92:112–224. https://doi.org/10.1016/j.pmatsci.2017.10.001

[8] Seabra M, Azevedo J, Araújo A et al (2016) Selective laser melting (SLM) and topology optimization for lighter aerospace componentes. Procedia Struct Integr 1:289–296. https://doi.org/10.1016/j.prostr.2016.02.039

[9] Loh GH, Pei E, Harrison D, Monzón MD (2018) An overview of functionally graded additive manufacturing. Addit Manuf 23:34–44. https://doi.org/10.1016/j.addma.2018.06.023

[10] Mahamood RM, Akinlabi ET (2015) Laser metal deposition of functionally graded Ti6Al4V/TiC. Mater Des 84:402–410. https://doi.org/10.1016/j.matdes.2015.06.135

[11] Tüzemen MÇ, Salamcı E, Ünal R (2022) Investigation of the relationship between flexural modulus of elasticity and functionally graded porous structures manufactured by AM. Mater Today Commun 31:103592

[12] Popovich VA, Borisov EV, Popovich AA et al (2017) Functionally graded Inconel 718 processed by additive manufacturing: crystallographic texture, anisotropy of microstructure and mechanical properties. Mater Des 114:441–449. https://doi.org/10.1016/j.matdes.2016.10.075

[13] Tascioglu E, Karabulut Y, Kaynak Y (2020) Influence of heat treatment temperature on the microstructural, mechanical, and wear behavior of 316L stainless steel fabricated by laser powder bed additive manufacturing. Int J Adv Manuf Technol 107:1947. https://doi.org/10.1007/s00170-020-05115-1

[14] Yasa E, Deckers J, Kruth JP (2011) The investigation of the influence of laser re-melting on density, surface quality and microstructure of selective laser melting parts. Rapid Prototyp J 17:312–327. https://doi.org/10.1108/13552541111156450

[15] Li C, Liu ZY, Fang XY, Guo YB (2018) Residual stress in metal additive manufacturing. Procedia CIRP 71:348–353. https://doi.org/10.1016/j.procir.2018.05.039

[16] Kok Y, Tan XP, Wang P et al (2018) Anisotropy and heterogeneity of microstructure and mechanical properties in metal additive manufacturing: a critical review. Mater Des 139:565–586. https://doi.org/10.1016/j.matdes.2017.11.021

[17] Khan HM, Karabulut Y, Kitay O et al (2020) Influence of the post-processing operations on surface integrity of metal components produced by laser powder bed fusion additive manufacturing: a review. Mach Sci Technol 25:118–176. https://doi.org/10.1080/10910344.2020.1855649

[18] Li W, Li S, Liu J et al (2016) Effect of heat treatment on AlSi10Mg alloy fabricated by selective laser melting: microstructure evolution, mechanical properties and fracture mechanism. Mater Sci Eng A 663:116–125. https://doi.org/10.1016/j.msea.2016.03.088

[19] Wang Y, Shi J (2020) Effect of hot isostatic pressing on nanoparticles reinforced AlSi10Mg produced by selective laser melting. Mater Sci Eng A. https://doi.org/10.1016/j.msea.2020.139570

[20] Amirkhanlou S, Ji S (2020) A review on high stiffness aluminum-based composites and bimetallics. Crit Rev Solid State Mater Sci 45:1–21. https://doi.org/10.1080/10408436.2018.1485550

[21] Wang Z, Qu RT, Scudino S et al (2015) Hybrid nanostructured aluminum alloy with super-high strength. NPG Asia Mater 7:1–8. https://doi.org/10.1038/am.2015.129

[22] Zhang Y, Guo Y, Chen Y et al (2019) Ultrasonic-assisted laser metal deposition of the Al 4047alloy. Metals (Basel) 9:1–15. https://doi.org/10.3390/met9101111

[23] Niu F, Wu D, Ma G et al (2015) Nanosized microstructure of Al2O3-ZrO2 (Y2O3) eutectics fabricated by laser engineered net shaping. Scr Mater 95:39–41. https://doi.org/10.1016/j.scriptamat.2014.09.026

[24] Li J, Wang HM (2010) Microstructure and mechanical properties of rapid directionally solidified Ni-base superalloy Rene'41 by laser melting deposition manufacturing. Mater Sci Eng A 527:4823–4829. https://doi.org/10.1016/j.msea.2010.04.062

[25] Hu Y, Cong W, Wang X et al (2018) Laser deposition-additive manufacturing of TiB-Ti composites with novel three-dimensional quasi-continuous network microstructure: effects on strengthening and toughening. Compos Part B Eng 133:91–100. https://doi.org/10.1016/j.compositesb.2017.09.019

[26] Emamian A, Alimardani M, Khajepour A (2014) Effect of cooling rate and laser process parameters on additive manufactured Fe-Ti-C metal matrix composites microstructure and carbide morphology. J Manuf Process 16:511–517. https://doi.org/10.1016/j.jmapro.2014.07.002

[27] Koczak MJ, Premkumar MK (1993) Emerging technologies for the in-situ production of MMCs. Jom 45:44–48. https://doi.org/10.1007/BF03223365

[28] He X, Zhang YZ, Mansell JP, Su B (2008) Zirconia toughened alumina ceramic foams for potential bone graft applications: fabrication, bioactivation, and cellular responses. J Mater Sci Mater Med 19:2743–2749. https://doi.org/10.1007/s10856-008-3401-x

[29] Mandal N, Doloi B, Mondal B (2013) Predictive modeling of surface roughness in high speed machining of AISI 4340 steel using yttria stabilized zirconia toughened alumina turning insert. Int J Refract Met Hard Mater 38:40–46. https://doi.org/10.1016/j.ijrmhm.2012.12.007

[30] Miracle DB (2005) Metal matrix composites–From science to technological significance. Compos Sci Technol 65:2526–2540. https://doi.org/10.1016/j.compscitech.2005.05.027

[31] Scudino S, Liu G, Sakaliyska M et al (2009) Powder metallurgy of Al-based metal matrix composites reinforced with β-Al3Mg2 intermetallic particles: analysis and modeling of mechanical properties. Acta Mater 57:4529–4538. https://doi.org/10.1016/j.actamat.2009.06.017

[32] Ghomashchi MR, Vikhrov A (2000) Squeeze casting: an overview. J Mater Process Technol 101:1–9. https://doi.org/10.1016/S0924-0136(99)00291-5

[33] Cyboroń J, Karolus M, Putyra P et al (2016) Structure properties of AlSi7Mg/SiC composite produced by stir casting method. Acta Phys Pol A 130:969–971. https://doi.org/10.12693/APhysPolA.130.969

[34] Dehghan Hamedan A, Shahmiri M (2012) Production of A356–1wt% SiC nanocomposite by the modified stir casting method. Mater Sci Eng A 556:921–926. https://doi.org/10.1016/j.msea.2012.07.093

[35] Rosso M (2006) Ceramic and metal matrix composites: routes and properties. J Mater Process Technol 175:364–375. https://doi.org/10.1016/j.jmatprotec.2005.04.038

[36] Zhang B, Zheng XL, Tokura H, Yoshikawa M (2003) Grinding induced damage in ceramics. J Mater Process Technol 132:353–364. https://doi.org/10.1016/S0924-0136(02)00952-4

[37] Dadbakhsh S, Mertens R, Hao L et al (2019) Selective laser melting to manufacture "in situ" metal matrix composites: a review. Adv Eng Mater 21:1–18. https://doi.org/10.1002/adem.201801244

[38] Dinda GP, Dasgupta AK, Mazumder J (2012) Evolution of microstructure in laser deposited Al–11.28% Si alloy. Surf Coatings Technol 206:2152–2160

[39] Dinda GP, Dasgupta AK, Bhattacharya S et al (2013) Microstructural characterization of laser-deposited Al 4047 alloy. Metall Mater Trans A 44:2233–2242

[40] Bhavar V, Kattire P, Patil V, et al (2017) A review on powder bed fusion technology of metal additive manufacturing. Addit Manuf Handb 251–253

[41] Levy GN (2010) The role and future of the Laser technology in the Additive Manufacturing environment. Phys Procedia 5:65–80. https://doi.org/10.1016/j.phpro.2010.08.123

[42] Olakanmi EO, Cochrane RF, Dalgarno KW (2015) A review on selective laser sintering/melting (SLS/SLM) of aluminium alloy powders: processing, microstructure, and properties. Prog Mater Sci 74:401–477. https://doi.org/10.1016/j.pmatsci.2015.03.002

[43] Agarwala M, Bourell D, Beaman J et al (1995) Direct selective laser sintering of metals. Rapid Prototyp J 1:26–36. https://doi.org/10.1108/13552549510078113

[44] Yap CY, Chua CK, Dong ZL et al (2015) Review of selective laser melting: materials and applications. Appl Phys Rev. https://doi.org/10.1063/1.4935926

[45] Lachmayer R, Zghair YA, Klose C, Nürnberger F (2016) Introducing selective laser melting to manufacture machine elements. In: DS 84: Proceedings of the DESIGN 2016 14th international design conference. pp 831–842

[46] Samanta A, Wang Q, Ding H (2018) A novel selective laser melting process for glass fiber-reinforced metal matrix composites. Manuf Lett 18:27–30. https://doi.org/10.1016/j.mfglet.2018.09.006

[47] Shen N, Samanta A, Wang Q, Ding H (2017) Selective laser melting of fiber-reinforced glass composites. Manuf Lett 14:6–9. https://doi.org/10.1016/j.mfglet.2017.09.001

[48] Fereiduni E, Ghasemi A, Elbestawi M (2019) Selective laser melting of hybrid ex-situ/in-situ reinforced titanium matrix composites: laser/powder interaction, reinforcement formation mechanism, and non-equilibrium microstructural evolutions. Mater Des 184:108185. https://doi.org/10.1016/j.matdes.2019.108185

[49] Zhai W, Zhu Z, Zhou W et al (2020) Selective laser melting of dispersed TiC particles strengthened 316L stainless steel. Compos Part B Eng 199:108291. https://doi.org/10.1016/j.compositesb.2020.108291

[50] Fereiduni E, Ghasemi A, Elbestawi M (2020) Selective laser melting of aluminum and titanium matrix composites: recent progress and potential applications in the aerospace industry. Aerospace. https://doi.org/10.3390/AEROSPACE7060077

[51] Zhou W, Sun X, Kikuchi K et al (2018) Carbon nanotubes as a unique agent to fabricate nanoceramic/metal composite

powders for additive manufacturing. Mater Des 137:276–285. https://doi.org/10.1016/j.matdes.2017.10.034

[52] Li M, Fang A, Martinez-Franco E et al (2019) Selective laser melting of metal matrix composites: feedstock powder preparation by electroless plating. Mater Lett 247:115–118. https://doi.org/10.1016/j.matlet.2019.03.092

[53] Aksoy A, Ünal R (2006) Effects of gas pressure and protrusion length of melt delivery tube on powder size and powder morphology of nitrogen gas atomised tin powders. Powder Metall. https://doi.org/10.1179/174329006X89425

[54] Ünal R (2007) Investigation on metal powder production efficiency of new convergent divergent nozzle in close coupled gas atomisation. Powder Metall 50:302–306. https://doi.org/10.1179/174329007X189595

[55] Chen G, Zhao SY, Tan P et al (2018) A comparative study of Ti-6Al-4V powders for additive manufacturing by gas atomization, plasma rotating electrode process and plasma atomization. Powder Technol 333:38–46. https://doi.org/10.1016/j.powtec.2018.04.013

[56] Yurtkuran E, Ünal R (2020) Numerical and experimental investigation on the effects of a nozzle attachment to plasma torches for plasma atomization. Plasma Chem Plasma Process 40:1127–1144. https://doi.org/10.1007/s11090-020-10095-x

[57] Yurturan E, Ünal R (2022) Theoretical and experimental investigation of Tialloy powder production using low-power plasma torches. Trans Nonferrous Met Soc China 32:175–191

[58] Tang S, Ummethala R, Suryanarayana C et al (2021) Additive manufacturing of aluminum-based metal matrix composites—A Review. Adv Eng Mater 23:1–17. https://doi.org/10.1002/adem.202100053

[59] Han Q, Setchi R, Evans SL (2016) Synthesis and characterisation of advanced ball-milled Al-Al2O3 nanocomposites for selective laser melting. Powder Technol 297:183–192. https://doi.org/10.1016/j.powtec.2016.04.015

[60] Riener K, Albrecht N, Ziegelmeier S et al (2020) Influence of particle size distribution and morphology on the properties of the powder feedstock as well as of AlSi10Mg parts produced by laser powder bed fusion (LPBF). Addit Manuf 34:101286. https://doi.org/10.1016/j.addma.2020.101286

[61] Wang R, Xi L, Ding K et al (2022) Powder preparation during ball milling and laser additive manufacturing of aluminum matrix nanocomposites: powder properties, processability and mechanical property. Adv Powder Technol 33:103687. https://doi.org/10.1016/j.apt.2022.103687

[62] Dadbakhsh S, Hao L (2012) Effect of Al alloys on selective laser melting behaviour and microstructure of in situ formed particle reinforced composites. J Alloys Compd 541:328–334. https://doi.org/10.1016/j.jallcom.2012.06.097

[63] Xia M, Liu A, Wang H et al (2019) Microstructure evolution and its effect on mechanical response of the multi-phase reinforced Ti-based composites by laser powder-bed fusion. J Alloys Compd 782:506–515. https://doi.org/10.1016/j.jallcom.2018.12.182

[64] Chen H, Gu D, Deng L et al (2020) Laser additive manufactured high-performance Fe-based composites with unique strengthening structure. J Mater Sci Technol. https://doi.org/10.1016/j.jmst.2020.04.011

[65] Chen H, Gu D, Kosiba K et al (2020) Achieving high strength and high ductility in WC-reinforced iron-based composites by laser additive manufacturing. Addit Manuf 35:101195. https://doi.org/10.1016/j.addma.2020.101195

[66] Gu D, Shen Y, Lu Z (2009) Microstructural characteristics and formation mechanism of direct laser-sintered Cu-based alloys reinforced with Ni particles. Mater Des 30:2099–2107. https://doi.org/10.1016/j.matdes.2008.08.036

[67] Gu D, Shen Y (2008) Direct laser sintered WC-10Co/Cu nanocomposites. Appl Surf Sci 254:3971–3978. https://doi.org/10.1016/j.apsusc.2007.12.028

[68] Zhang Z, Han Q, Yang S et al (2021) Laser powder bed fusion of advanced submicrometer TiB2 reinforced high-performance Ni-based composite. Mater Sci Eng A 817:141416. https://doi.org/10.1016/j.msea.2021.141416

[69] Kaczmar JW, Pietrzak K, Wlosiński W (2000) Production and application of metal matrix composite materials. J Mater Process Technol 106:58–67. https://doi.org/10.1016/S0924-0136(00)00639-7

[70] Han Q, Setchi R, Lacan F et al (2017) Selective laser melting of advanced Al-Al2O3 nanocomposites: simulation, microstructure and mechanical properties. Mater Sci Eng A 698:162–173. https://doi.org/10.1016/j.msea.2017.05.061

[71] Gao C, Wang Z, Xiao Z et al (2020) Selective laser melting of TiN nanoparticle-reinforced AlSi10Mg composite: microstructural, interfacial, and mechanical properties. J Mater Process Technol 281:116618. https://doi.org/10.1016/j.jmatprotec.2020.116618

[72] Dai D, Gu D (2016) Influence of thermodynamics within molten pool on migration and distribution state of reinforcement during selective laser melting of AlN/AlSi10Mg composites. Int J Mach Tools Manuf 100:14–24. https://doi.org/10.1016/j.ijmachtools.2015.10.004

[73] Li XP, Ji G, Chen Z et al (2017) Selective laser melting of nano-TiB2 decorated AlSi10Mg alloy with high fracture

strength and ductility. Acta Mater 129:183–193. https://doi.org/10.1016/j.actamat.2017.02.062

[74] Jiang L, Li Z, Fan G et al (2012) The use of flake powder metallurgy to produce carbon nanotube (CNT)/aluminum composites with a homogenous CNT distribution. Carbon N Y 50:1993–1998. https://doi.org/10.1016/j.carbon.2011.12.057

[75] Kusoglu IM, Gökce B, Barcikowski S (2020) Use of (nano-)additives in laser powder bed fusion of Al powder feedstocks: research directions within the last decade. Procedia CIRP 94:11–16. https://doi.org/10.1016/j.procir.2020.09.003

[76] Nayim SMTI, Hasan MZ, Seth PP et al (2020) Effect of CNT and TiC hybrid reinforcement on the micro-mechano-tribo behaviour of aluminium matrix composites. Mater Today Proc 21:1421–1424. https://doi.org/10.1016/j.matpr.2019.08.203

[77] Nair SV, Tien JK, Bates RC (1985) SiC-reinforced aluminium metal matrix composites. Int Met Rev 30:275–290. https://doi.org/10.1179/imtr.1985.30.1.275

[78] Chen AL, Arai Y, Tsuchida E (2005) An experimental study on effect of thermal cycling on monotonic and cyclic response of cast aluminium alloy-SiC particulate composites. Compos Part B Eng 36:319–330. https://doi.org/10.1016/j.compositesb.2004.11.006

[79] Yang Z, Lu Z (2013) Atomistic simulation of the mechanical behaviors of co-continuous Cu/SiC nanocomposites. Compos Part B Eng 44:453–457. https://doi.org/10.1016/j.compositesb.2012.04.010

[80] Umanath K, Palanikumar K, Selvamani ST (2013) Analysis of dry sliding wear behaviour of Al6061/SiC/Al2O 3 hybrid metal matrix composites. Compos Part B Eng 53:159–168. https://doi.org/10.1016/j.compositesb.2013.04.051

[81] Li X, Zhang K, Konietzky H et al (2020) Experimental study on the dynamic mechanical behaviors of silicon carbide ceramic after thermal shock. Nucl Mater Energy 24:100774. https://doi.org/10.1016/j.nme.2020.100774

[82] Nastic A, Merati A, Bielawski M et al (2015) Instrumented and vickers indentation for the characterization of stiffness, hardness and toughness of zirconia toughened Al_2O_3 and SiC Armor. J Mater Sci Technol 31:773–783. https://doi.org/10.1016/j.jmst.2015.06.005

[83] Du Y, Zhang P, Zhang W, Wang Y (2018) Distribution of SiC particles in semisolid electromagnetic-mechanical stir-casting Al-SiC composite. China Foundry 15:351–357

[84] Anandkumar R, Almeida A, Colaço R et al (2007) Microstructure and wear studies of laser clad Al-Si/SiC(p) composite coatings. Surf Coatings Technol 201:9497–9505. https://doi.org/10.1016/j.surfcoat.2007.04.003

[85] Lloyd DJ (1994) Particle reinforced aluminium and magnesium matrix composites. Int Mater Rev 39:1–23. https://doi.org/10.1179/imr.1994.39.1.1

[86] Ibrahim IA, Mohamed FA, Lavernia EJ (1991) Particulate reinforced metal matrix composites—A review. J Mater Sci 26:1137–1156. https://doi.org/10.1007/BF00544448

[87] Astfalck LC, Kelly GK, Li X, Sercombe TB (2017) On the breakdown of SiC during the selective laser melting of aluminum matrix composites. Adv Eng Mater 19:1–6. https://doi.org/10.1002/adem.201600835

[88] Xue G, Ke L, Zhu H et al (2019) Influence of processing parameters on selective laser melted SiCp/AlSi10Mg composites: densification, microstructure and mechanical properties. Mater Sci Eng A. https://doi.org/10.1016/j.msea.2019.138155

[89] Ghosh SK, Saha P, Kishore S (2010) Influence of size and volume fraction of SiC particulates on properties of ex situ reinforced Al-4.5Cu-3Mg metal matrix composite prepared by direct metal laser sintering process. Mater Sci Eng A 527:4694–4701. https://doi.org/10.1016/j.msea.2010.03.108

[90] Gu D, Chang F, Dai D (2015) Selective laser melting additive manufacturing of novel aluminum based composites with multiple reinforcing phases. J Manuf Sci Eng Trans ASME 137:1–11. https://doi.org/10.1115/1.4028925

[91] Xue G, Ke L, Liao H et al (2020) Effect of SiC particle size on densification behavior and mechanical properties of SiCp/AlSi10Mg composites fabricated by laser powder bed fusion. J Alloys Compd. https://doi.org/10.1016/j.jallcom.2020.156260

[92] Chang F, Gu D, Dai D, Yuan P (2015) Selective laser melting of in-situ Al4SiC4 + SiC hybrid reinforced Al matrix composites: influence of starting SiC particle size. Surf Coatings Technol 272:15–24. https://doi.org/10.1016/j.surfcoat.2015.04.029

[93] Wang M, Song B, Wei Q, Shi Y (2019) Improved mechanical properties of AlSi7Mg/nano-SiCp composites fabricated by selective laser melting. J Alloys Compd 810:151926. https://doi.org/10.1016/j.jallcom.2019.151926

[94] Yu WH, Sing SL, Chua CK et al (2019) Particle-reinforced metal matrix nanocomposites fabricated by selective laser melting: a state of the art review. Prog Mater Sci 104:330–379. https://doi.org/10.1016/j.pmatsci.2019.04.006

[95] Gu D, Yang Y, Xi L et al (2019) Laser absorption behavior of randomly packed powder-bed during selective laser melting of SiC and TiB2 reinforced Al matrix composites.

Opt Laser Technol. https://doi.org/10.1016/j.optlastec.2019.105600

[96] Gu D, Hagedorn YC, Meiners W et al (2012) Densification behavior, microstructure evolution, and wear performance of selective laser melting processed commercially pure titanium. Acta Mater 60:3849–3860. https://doi.org/10.1016/j.actamat.2012.04.006

[97] Wang Z, Zhuo L, Yin E, Zhao Z (2021) Microstructure evolution and properties of nanoparticulate SiC modified AlSi10Mg alloys. Mater Sci Eng A. https://doi.org/10.1016/j.msea.2021.140864

[98] Wang L, zhi, Wang S, Wu J jiao, (2017) Experimental investigation on densification behavior and surface roughness of AlSi10Mg powders produced by selective laser melting. Opt Laser Technol 96:88–96. https://doi.org/10.1016/j.optlastec.2017.05.006

[99] Yang KV, Rometsch P, Jarvis T et al (2018) Porosity formation mechanisms and fatigue response in Al-Si-Mg alloys made by selective laser melting. Mater Sci Eng A 712:166–174. https://doi.org/10.1016/j.msea.2017.11.078

[100] Ribes H, Da Silva R, Suéry M, Bretheau T (1990) Effect of interfacial oxide layer in Al–SiC particle composites on bond strength and mechanical behaviour. Mater Sci Technol (United Kingdom) 6:621–628. https://doi.org/10.1179/mst.1990.6.7.621

[101] Zhang W, Zhu H, Hu Z, Zeng X (2017) Study on the Selective laser melting of AlSi10Mg. Jinshu Xuebao Acta Metall Sin 53:918–926. https://doi.org/10.11900/0412.1961.2016.00472

[102] Hadadzadeh A, Amirkhiz BS, Mohammadi M (2019) Contribution of Mg2Si precipitates to the strength of direct metal laser sintered AlSi10Mg. Mater Sci Eng A 739:295–300. https://doi.org/10.1016/j.msea.2018.10.055

[103] Tan Q, Zhang J, Mo N et al (2020) A novel method to 3D-print fine-grained AlSi10Mg alloy with isotropic properties via inoculation with LaB6 nanoparticles. Addit Manuf 32:101034. https://doi.org/10.1016/j.addma.2019.101034

[104] Suryawanshi J, Prashanth KG, Scudino S et al (2016) Simultaneous enhancements of strength and toughness in an Al-12Si alloy synthesized using selective laser melting. Acta Mater 115:285–294. https://doi.org/10.1016/j.actamat.2016.06.009

[105] Dai D, Gu D, Zhang H et al (2018) Influence of scan strategy and molten pool configuration on microstructures and tensile properties of selective laser melting additive manufactured aluminum based parts. Opt Laser Technol 99:91–100. https://doi.org/10.1016/j.optlastec.2017.08.015

[106] Narayanasamy R, Anandakrishnan V, Pandey KS (2008) Effect of geometric work-hardening and matrix work-hardening on workability and densification of aluminium-3.5% alumina composite during cold upsetting. Mater Des 29:1582–1599. https://doi.org/10.1016/j.matdes.2007.11.006

[107] Albiter A, Contreras A, Bedolla E, Perez R (2003) Structural and chemical characterization of precipitates in Al-2024/TiC composites. Compos Part A Appl Sci Manuf 34:17–24. https://doi.org/10.1016/S1359-835X(02)00259-2

[108] Mhadhbi M (2020) Titanium carbide: synthesis, properties and applications. Brill Eng 2:1–11. https://doi.org/10.36937/ben.2021.002.001

[109] Wang P, Eckert J, Prashanth K, gokuldoss, et al (2020) A review of particulate-reinforced aluminum matrix composites fabricated by selective laser melting. Trans Nonferrous Met Soc China 30(8):2001–2034

[110] Almangour B (2018) Additive manufacturing of emerging materials. Springer, Newyork

[111] Zhou Y, Wen S, Wang C et al (2019) Effect of TiC content on the Al-15Si alloy processed by selective laser melting: microstructure and mechanical properties. Opt Laser Technol. https://doi.org/10.1016/j.optlastec.2019.105719

[112] Gu D, Wang H, Chang F, et al (2014) Selective laser melting additive manufacturing of TiC/AlSi10Mg bulk-form nanocomposites with tailored microstructures and properties. In: Physics Procedia. pp 108–116

[113] Chen H, Gu D, Dai D et al (2017) Microstructure and composition homogeneity, tensile property, and underlying thermal physical mechanism of selective laser melting tool steel parts. Mater Sci Eng A 682:279–289. https://doi.org/10.1016/j.msea.2016.11.047

[114] Rodriguez MA, Stefan DK, Allen A, et al (2017) Microstructure and Thermal Properties of Selective Laser Melted AlSi10Mg Alloy. Sandia Natl Lab (SNL-NM), Albuquerque, NM (United States)

[115] Zhang Y, Zhang HL, Wu JH, Wang XT (2011) Enhanced thermal conductivity in copper matrix composites reinforced with titanium-coated diamond particles. Scr Mater 65:1097–1100. https://doi.org/10.1016/j.scriptamat.2011.09.028

[116] Vasantgadkar NA, Bhandarkar UV, Joshi SS (2010) A finite element model to predict the ablation depth in pulsed laser ablation. Thin Solid Films 519:1421–1430. https://doi.org/10.1016/j.tsf.2010.09.016

[117] Louvis E, Fox P, Sutcliffe CJ (2011) Selective laser melting of aluminium components. J Mater Process Technol 211:275–284. https://doi.org/10.1016/j.jmatprotec.2010.09.019

[118] Yuan P, Gu D, Dai D (2015) Particulate migration behavior and its mechanism during selective laser melting of TiC reinforced Al matrix nanocomposites. Mater Des 82:46–55. https://doi.org/10.1016/j.matdes.2015.05.041

[119] Zhou SY, Wang ZY, Su Y et al (2020) Effects of micron/submicron TiC on additively manufactured AlSi10Mg: a comprehensive study from computer simulation to mechanical and microstructural analysis. Jom 72:3693–3704. https://doi.org/10.1007/s11837-019-03984-w

[120] Lin TC, Cao C, Sokoluk M et al (2019) Aluminum with dispersed nanoparticles by laser additive manufacturing. Nat Commun 10:1–9. https://doi.org/10.1038/s41467-019-12047-2

[121] Gu DD, Meiners W, Wissenbach K, Poprawe R (2012) Laser additive manufacturing of metallic components: materials, processes and mechanisms. Int Mater Rev 57:133–164. https://doi.org/10.1179/1743280411Y.0000000014

[122] Gu D, Wang H, Dai D et al (2015) Densification behavior, microstructure evolution, and wear property of TiC nanoparticle reinforced AlSi10Mg bulk-form nanocomposites prepared by selective laser melting. J Laser Appl 27:S17003. https://doi.org/10.2351/1.4870877

[123] Gu D, Wang H, Chang F, et al (2014) Selective laser melting additive manufacturing of TiC/AlSi10Mg bulk-form nanocomposites with tailored microstructures and properties. In: Physics Procedia. Elsevier B.V., pp 108–116

[124] Arafune K, Hirata A (1999) Thermal and solutal marangoni convection in In-Ga-Sb system. J Cryst Growth 197:811–817. https://doi.org/10.1016/S0022-0248(98)01071-9

[125] Gu D, Wang H, Dai D et al (2015) Rapid fabrication of Al-based bulk-form nanocomposites with novel reinforcement and enhanced performance by selective laser melting. Scr Mater 96:25–28. https://doi.org/10.1016/j.scriptamat.2014.10.011

[126] Gu D, Shen Y (2007) Effects of dispersion technique and component ratio on densification and microstructure of multi-component Cu-based metal powder in direct laser sintering. J Mater Process Technol 182:564–573. https://doi.org/10.1016/j.jmatprotec.2006.09.026

[127] Simchi A (2006) Direct laser sintering of metal powders: mechanism, kinetics and microstructural features. Mater Sci Eng A 428:148–158. https://doi.org/10.1016/j.msea.2006.04.117

[128] Gu D, Wang H, Dai D (2016) Laser additive manufacturing of novel aluminum based nanocomposite parts: tailored forming of multiple materials. J Manuf Sci Eng Trans ASME 138:1–11. https://doi.org/10.1115/1.4030376

[129] Wang H, Gu D (2015) Nanometric TiC reinforced AlSi10Mg nanocomposites: powder preparation by high-energy ball milling and consolidation by selective laser melting. J Compos Mater 49:1639–1651. https://doi.org/10.1177/0021998314538870

[130] Zhong XL, Wong WLE, Gupta M (2007) Enhancing strength and ductility of magnesium by integrating it with aluminum nanoparticles. Acta Mater 55:6338–6344. https://doi.org/10.1016/j.actamat.2007.07.039

[131] Hassan SF, Gupta M (2005) Development of high performance magnesium nano-composites using nano-Al_2O_3 as reinforcement. Mater Sci Eng A 392:163–168. https://doi.org/10.1016/j.msea.2004.09.047

[132] Mohanty PS, Mazumder J (1998) Solidification behavior and microstructural evolution during laser beam-material interaction. Metall Mater Trans 29:1269–1279. https://doi.org/10.1007/s11663-998-0050-x

[133] Wang Y, Shi J (2020) Effect of post heat treatment on the microstructure and tensile properties of nano TiC particulate reinforced inconel 718 by selective laser melting. J Manuf Sci Eng Trans ASME 142:1–12. https://doi.org/10.1115/1.4046646

[134] Lorusso M, Aversa A, Manfredi D et al (2016) Tribological behavior of aluminum alloy AlSi10Mg-TiB2 composites produced by direct metal laser sintering (DMLS). J Mater Eng Perform 25:3152–3160. https://doi.org/10.1007/s11665-016-2190-5

[135] Liao H, Zhu H, Xue G, Zeng X (2019) Alumina loss mechanism of Al_2O_3-AlSi10 Mg composites during selective laser melting. J Alloys Compd 785:286–295. https://doi.org/10.1016/j.jallcom.2019.01.116

[136] Jue J, Gu D, Chang K, Dai D (2017) Microstructure evolution and mechanical properties of Al-Al_2O_3 composites fabricated by selective laser melting. Powder Technol 310:80–91. https://doi.org/10.1016/j.powtec.2016.12.079

[137] Li W, Yang Y, Liu J et al (2017) Enhanced nanohardness and new insights into texture evolution and phase transformation of TiAl/TiB2 in-situ metal matrix composites prepared via selective laser melting. Acta Mater 136:90–104

[138] Gao C, Wu W, Shi J et al (2020) Simultaneous enhancement of strength, ductility, and hardness of TiN/AlSi10Mg nanocomposites via selective laser melting. Addit Manuf. https://doi.org/10.1016/j.addma.2020.101378

[139] Gao C, Xiao Z, Liu Z et al (2019) Selective laser melting of nano-TiN modified AlSi10Mg composite powder with low laser reflectivity. Mater Lett 236:362–365. https://doi.org/10.1016/j.matlet.2018.10.126

[140] Turnbull D, Vonnegut B (1952) Nucleation catalysis. Ind Eng Chem 44:1292–1298

[141] Xi L, Gu D, Guo S et al (2020) Grain refinement in laser manufactured Al-based composites with TiB2 ceramic.

J Mater Res Technol 9:2611–2622. https://doi.org/10.1016/j.jmrt.2020.04.059

[142] Xiao YK, Bian ZY, Wu Y et al (2019) Effect of nano-TiB2 particles on the anisotropy in an AlSi10Mg alloy processed by selective laser melting. J Alloys Compd 798:644–655. https://doi.org/10.1016/j.jallcom.2019.05.279

[143] Xi L, Gu D, Lin K et al (2020) Effect of ceramic particle size on densification behavior, microstructure formation, and performance of TiB-reinforced Al-based composites prepared by selective laser melting. J Mater Res 35:559–570. https://doi.org/10.1557/jmr.2019.392

[144] Du Z, Chen HC, Tan MJ et al (2020) Effect of nAl2O3 on the part density and microstructure during the laser-based powder bed fusion of AlSi10Mg composite. Rapid Prototyp J 26:727–735. https://doi.org/10.1108/RPJ-05-2019-0136

[145] Xi L, Guo S, Gu D et al (2020) Microstructure development, tribological property and underlying mechanism of laser additive manufactured submicro-TiB2 reinforced Al-based composites. J Alloys Compd 819:152980. https://doi.org/10.1016/j.jallcom.2019.152980

[146] Li Y, Gu D, Zhang H, Xi L (2020) Effect of trace addition of ceramic on microstructure development and mechanical properties of selective laser melted AlSi10Mg alloy. Chin J Mech Eng. https://doi.org/10.1186/s10033-020-00448-0

[147] Xi L, Wang P, Prashanth KG et al (2019) Effect of TiB2 particles on microstructure and crystallographic texture of Al-12Si fabricated by selective laser melting. J Alloys Compd 786:551–556. https://doi.org/10.1016/j.jallcom.2019.01.327

[148] Sanaty-Zadeh A (2012) Comparison between current models for the strength of particulate-reinforced metal matrix nanocomposites with emphasis on consideration of Hall-Petch effect. Mater Sci Eng A 531:112–118. https://doi.org/10.1016/j.msea.2011.10.043

[149] Wang W, Bai X, Zhang L et al (2022) Additive manufacturing of Csf/SiC composites with high fiber content by direct ink writing and liquid silicon infiltration. Ceram Int 48:3895–3903. https://doi.org/10.1016/j.ceramint.2021.10.176

[150] Liu X, Zou B, Xing H, Huang C (2020) The preparation of ZrO2-Al_2O_3 composite ceramic by SLA-3D printing and sintering processing. Ceram Int 46:937–944. https://doi.org/10.1016/j.ceramint.2019.09.054

[151] Li S, Zhang Y, Zhao T et al (2020) Additive manufacturing of SiBCN/Si 3 N 4 w composites from preceramic polymers by digital light processing. RSC Adv 10:5681–5689

[152] Fu H, Zhu W, Xu Z et al (2019) Effect of silicon addition on the microstructure, mechanical and thermal properties of Cf/SiC composite prepared via selective laser sintering. J Alloys Compd 792:1045–1053. https://doi.org/10.1016/j.jallcom.2019.04.129

[153] Zhang H, Yang Y, Hu K et al (2020) Stereolithography-based additive manufacturing of lightweight and high-strength Cf/SiC ceramics. Addit Manuf 34:101199. https://doi.org/10.1016/j.addma.2020.101199

[154] Xie H, Zhang J, Li F et al (2021) Selective laser melting of SiCp/Al composites: densification, microstructure, and mechanical and tribological properties. Ceram Int 47:30826–30837. https://doi.org/10.1016/j.ceramint.2021.07.263

[155] Zhao X, Gu D, Ma C et al (2019) Microstructure characteristics and its formation mechanism of selective laser melting SiC reinforced Al-based composites. Vacuum 160:189–196. https://doi.org/10.1016/j.vacuum.2018.11.022

[156] He P, Kong H, Liu Q et al (2021) Elevated temperature mechanical properties of TiCN reinforced AlSi10Mg fabricated by laser powder bed fusion additive manufacturing. Mater Sci Eng A 811:141025. https://doi.org/10.1016/j.msea.2021.141025

[157] Wu L, Zhao Z, Bai P et al (2020) Wear resistance of graphene nano-platelets (GNPs) reinforced AlSi10Mg matrix composite prepared by SLM. Appl Surf Sci 503:144156. https://doi.org/10.1016/j.apsusc.2019.144156

[158] Luo S, Li R, He P et al (2021) Investigation on the microstructure and mechanical properties of CNTs-AlSi10Mg composites fabricated by selective laser melting. Materials (Basel) 14:1–15. https://doi.org/10.3390/ma14040838

[159] Zhang D, Yi D, Wu X et al (2022) SiC reinforced AlSi10Mg composites fabricated by selective laser melting. J Alloys Compd. https://doi.org/10.1016/j.jallcom.2021.162365

[160] Zhang J, Li F, Zhu Q, Zhang H (2019) Preparation of silicon carbide reinforced aluminium matrix composites (SiC/Al) by selective laser melting. IOP Conf Ser Mater Sci Eng. https://doi.org/10.1088/1757-899X/678/1/012015

[161] Xi LX, Zhang H, Wang P et al (2018) Comparative investigation of microstructure, mechanical properties and strengthening mechanisms of Al-12Si/TiB2 fabricated by selective laser melting and hot pressing. Ceram Int 44:17635–17642. https://doi.org/10.1016/j.ceramint.2018.06.225

[162] Gao C, Liu Z, Xiao Z et al (2021) Effect of heat treatment on SLM-fabricated TiN/AlSi10Mg composites: microstructural evolution and mechanical properties. J Alloys Compd 853:156722. https://doi.org/10.1016/j.jallcom.2020.156722

[163] Han Q, Geng Y, Setchi R et al (2017) Macro and nanoscale wear behaviour of Al-Al_2O_3 nanocomposites fabricated by selective laser melting. Compos Part B Eng 127:26–35. https://doi.org/10.1016/j.compositesb.2017.06.026